To appear: Physics of Fluids

Dynamics of Probability Density Functions for Decaying Passive Scalars in Periodic Velocity Fields

Roberto Camassa
Neil Martinsen-Burrell
Richard M. McLaughlin
Department of Mathematics
University of North Carolina, Chapel Hill, NC, 27599

June 28, 2007

Abstract

The probability density function (PDF) for a decaying passive scalar advected by a deterministic, periodic, incompressible fluid flow is numerically studied using a variety of random and coherent initial scalar fields. We establish the dynamic emergence at large Péclet numbers of a broad-tailed PDF for the scalar initialized with a Gaussian random measure, and further explore a rich parameter space involving scales of the initial scalar field and the geometry of the flow. We document that the dynamic transition of the PDF to a broad tailed distribution is similar for shear flows and time-varying non-sheared flows with positive Lyapunov exponent, thereby showing that chaos in the particle trajectories is not essential to observe intermittent scalar signals. The role of the initial scalar field is carefully explored. The long time PDF is sensitive to the scale of the initial data. For shear flows we show that heavy-tailed PDFs appear only when the initial field has sufficiently small-scale variation. We also connect geometric features of the scalar field with the shape of the PDFs. We document that the PDF is constructed by a subtle balance between spatial regions of strong *and* weak shear in conjunction with the presence of

small-scale scalar variation within the weak shear regions. For cellular flows we document a lack of self-similarity in the PDFs when periodic time dependence is present, in contrast to the self-similar decay for time independent flow. Finally we analyze the behavior of the PDFs for coherent initial fields and the parametric dependence of the variance decay rate on the Péclet number and the initial wavenumber of the scalar field.

I Introduction

The mixing and transport of numerous environmental scalars (salt, temperature, ozone, etc) provide important information regarding the behavior of our environment. Whether inert or reacting, active or passive, the distribution of tracers is directly affected by the motion of the fluids in which these scalars are immersed. The direct problem of predicting properties of the evolving scalars even for prescribed fluid motions is difficult. An intense scientific effort has been focused upon attempting to characterize the passive problem for a scalar diffusing in the presence of a given incompressible fluid flow, from cataloging bulk mixing properties important to sub-grid scale phenomena arising in numerical weather prediction, to the detailed monitoring of moments and distribution of scalar signals in the environment which indicate the stoichiometric properties of the atmosphere. Mathematically, this problem is challenging due to statistical closure problems arising from the variable coefficient fluid advection.

Through exhaustive experimental, empirical, theoretical, and mathematical study, a somewhat incomplete picture has arisen in which it is recognized that frequently the distribution of a passive scalar (whether distribution of values, or distribution in ensemble) is seen to be non-Gaussian, emphasized by a heavy tail which contains significant probability for large fluctuation many standard deviations away from the mean, especially when advective affects dominate diffusive effects (high Péclet numbers). Examples are ubiquitous, to list a few: the Chicago experiments[1] established that, in high Rayleigh convection single point measurements of the thermal field exhibit a time series with values roughly following a Gaussian distribution for low Rayleigh numbers, but follow an exponential distribution for high Rayleigh numbers. Sparling analyzed[2] aircraft measurements for stratospheric chemicals and documented strong non-Gaussianity in these measurements which follow stretched exponential distributions. Similar behavior has been observed in the ocean in towed measurements of water properties as reported by Ferrari and Rudnick.[3]

We are particularly motivated by the experimental data in this case. In both the ocean[3] and the atmosphere[2] scalar values were measured over time as the measuring platform moved through the surrounding fluid. The measured values were then considered as samples from a distribution of possible scalar values and histograms were constructed to approximate the distribution of scalar values over space. These fluid flows are temporally varying

and spatially inhomogeneous, yet due to the sparsity of data collected it makes sense to consider the aggregated measurements as being drawn from some underlying distribution of scalar values. While this process of measurement and aggregation is fundamentally different than the classical situation of time-series analysis where the measured values at a single location are considered to follow some distribution, it is not *a priori* invalid. Rather the analysis presented here in terms of probability distribution functions for measured passive scalar values respects the content of observations that have been made. Attempts to interpret these observations have led to fundamental questions regarding the physical mechanisms responsible for setting up these heavy-tailed distributions. Firstly, given a prescribed fluid advection, what is the inherited distribution of scalar, either in value, or in ensemble? Secondly, given an observed passively transported scalar PDF, what can be said about the fluid advection responsible for that PDF? In this paper we provide partial answers to these questions. We document that the emergence of non-Gaussian, heavy-tailed PDFs can be attributed to the interplay of three key ingredients: the presence of sufficient small-scale tracer variations, the presence in the fluid flow of regions of strong shear, and the presence of shear free regions.

Given the intrinsically stochastic nature of fluid turbulence, much effort has been devoted to exploring these questions for a variety of stochastic fluid flows, the majority of which are taken to be Gaussian random fields in space-time. For such random flows, a host of theoretical results have helped to understand the origin of non-Gaussianity in scalar signals.[4–22] Different types of stochastic flows have been shown to give rise to heavy tailed scalar distribution functions, some involving positive Lyapunov exponents,[9,16,23] and others with pure shear flows having no positive Lyapunov exponent.[5–7,11,14,15,20] The basic picture for such studies is that the PDF for large scalar fluctuations is composed of values associated with anomalously rare coherent fluid stretching events which outlive their incoherent counterparts under the action of diffusion. A natural question is to isolate the essential role played by stochasticity in these studies. To that end, Bourlioux and Majda[19] exhibited that a passive scalar advected by either a deterministic or a random shear layer while diffusing in the presence of a large scale scalar gradient could also develop a non-Gaussian PDF, with large probability of large deviations over a wide range of scalar values.

The problem of passive scalar advection-diffusion has also been extensively studied in the context of chaotic advection,[24,25] which focuses on the

dynamic properties of the underlying fluid flow to explain the scalar distributions. The discovery of persistent spatial patterns in chaotic advection experiments[26] led to the study of those patterns, known as "strange eigenmodes".[18,27–29] Much of this literature focuses on the rate of decay of the scalar variance[30–35] and the behavior of that rate as the diffusivity vanishes. We will not concern ourselves with this question in this study, except to mention that the relation between the spatial scales of the fluid flow and the scalar field are important there as they will be here.[35] A more directly relevant subset of this literature is that on the limiting probability distributions[12,18,36,37] of passive scalars. Sinai and Yakhot[12] gave an equation for the limiting, stationary probability distribution of scalar values (if one exists) in terms of the conditional scalar dissipation rate. While this theory applies whenever the PDF is stationary, it is not predictive because the conditional dissipation rate cannot in general be computed *a priori*. Sukhatme[37] applied the Sinai-Yakhot theory to a family of lattice advection diffusion simulations.

The purpose of the present study is to present a series of highly resolved, long time numerical experiments designed to explore the distribution of scalar values for a decaying passive scalar, initiated with either random or coherent initial data, and advected by a deterministic, periodic, incompressible fluid flow. Through these simulations, we observe the longest lived, slowest decaying eigenmode, which retains features of both the initial random scalar field, and the prescribed fluid flow. The probability distribution functions (PDFs) will be defined in terms of the instantaneous *spatial* distribution of scalar values (generalizing to multiple dimensions those considered by Bourlioux and Majda[19]) in contrast to more familiar ensemble or time averaged constructions. These numerical results should be taken not to discount the more complicated fluid motions and complicated analyses which identify the limiting PDF, but rather to present a documentation of the heavy-tailed distributions which may arise from simple fluid flows in order to give improved interpretation of empirically measured PDFs. However, these numerical results should reinforce the fact that chaotic advection is *not* a necessary condition for the development of heavy tails.

We document through a series of flows with increasing complexity (shear, cellular, and time varying periodic perturbations of cellular flows) the scalar dynamics which give rise to heavy-tailed PDFs even for these simple fluid flows. Heavy tails are seen to arise whenever a balance between regions of strong and weak shear exists provided the initial conditions contain significant variability on small length scales. Thus, we present a list of mechanisms

that together can generate scalar distributions with significant intermittency. These mechanisms provide insight into possible sources of intermittency for more complicated flows as well. Further, these long time, high resolution simulations for the idealized flow models we consider are expected to provide useful benchmarks for other more complicated physical systems, such as arising in the modeling of oceanic mixing, where high Peclet numbers and long non-dimensional times such as those considered here are common.

The paper is organized as follows. Section II gives an introduction to probability density functions for passive scalars. In Section III we explore the development of non-Gaussian PDFs for several different types of fluid flows with multi-mode Gaussian random initial data, with the primary purpose of studying geometric flow structures responsible for the development of a heavy tailed PDF. We first explore steady shear layers in detail, and document an important competition between regions of strong shear and shear-free regions that is responsible for the development of a PDF resembling a stretched exponential distribution. By comparing shear flows with different sizes of these two regions we argue that, provided the length scale of initial scalar fluctuations is sufficiently small relative to size of the strain-free region, and provided that the fluid flow possesses additionally regions of strong strain, the PDF will stretch into a broad distribution strongly resembling a stretched exponential distribution.

In turn, we consider the PDF evolution for steady, and unsteady cellular flows and exhibit that this mechanism for shear layers persists for non-shear layers. In this context, we explore the Péclet number dependencies, and illustrate that a role of increasing Péclet number leads to scalar fields with "deep canyon" structures, and the binning of such scalar fields gives rise to broader PDFs than the associated low Péclet number counterparts. Lastly, in Section IV we focus upon the PDF evolution in both shear and cellular flows which results from coherent, single mode initial data. These cases show stronger memory of the initial scales than those with random initial data and they also have very clean PDF evolution to a stationary state resembling a stretched exponential distribution.

II Probability Density Functions for Scalar Fields

The probability density function is a common way of describing the density of values that a field takes on. Apart from its original use in probability theory (thus the name), the PDF is also a useful if unorthodox way to describe the values taken on by a specified function. For a space A and a measure μ with $\mu(A) < \infty$ and a function $f : A \to \mathbb{R}$, let

$$\mathrm{CDF}_f(z) := \frac{\mu\left(f^{-1}\left((-\infty, z]\right)\right)}{\mu(A)}$$

be the *cumulative distribution function* of f. Then define

$$\mathrm{PDF}_f(z) := \frac{\mathrm{d}}{\mathrm{d}z}\mathrm{CDF}_f(z), \tag{1}$$

as the *probability distribution function* of f. Thus, $\mathrm{PDF}_f(z)dz$ is the fraction of the space A where f takes on values in $(z, z+\mathrm{d}z]$. For fields f whose values are given by realizations of a random variable, the PDF of the function f is the same as that of the random variable. For specified functions f, the PDF can be computed analytically.

For example, if $f(x) = \sin x$, $A = [-\pi/2, \pi/2]$ and μ is the Lebesgue measure, then $\mathrm{CDF}_f(z) = (\sin^{-1} z)/\pi + 1/2$ for $-1 \le z \le 1$, and it is 0 or 1 respectively for $z < -1$ or $z > 1$. The corresponding PDF is therefore

$$\mathrm{PDF}_f(z) = \frac{1}{\pi}(1 - z^2)^{-1/2}, \qquad -1 \le z \le 1 \tag{2}$$

and 0 otherwise. Note that even in this simple example, the CDF is not everywhere differentiable and thus the PDF is singular for $z = \pm 1$.

As a further example, consider $f(x, y) = \sin x \sin y$ with $A = [0, 2\pi)^2$ and μ again the Lebesgue measure. The CDF for this function is the area enclosed by the level surfaces of f. These can be also viewed as trajectories of a simple dynamical system where f is interpreted as a Hamiltonian (or alternatively, a stream function for fluid particles):

$$\dot{x} = f_y\,, \qquad \dot{y} = -f_x\,.$$

With this in mind, the CDF, being the area enclosed by trajectories, becomes the action variable I and so

$$\frac{\mathrm{d}f}{\mathrm{d}I} = \Omega(I)$$

is the frequency of revolution for each trajectory identified by a constant value of f. Its reciprocal gives the PDF, which then coincides with the period of each closed orbit identified by a constant value of the Hamiltonian, $f = z$. The period can be computed in terms of elliptic integrals[38] to give the PDF

$$\mathrm{PDF}_f(z) = \frac{2}{\pi^2} K(\sqrt{1-z^2}), \qquad -1 \le z \le 1, \tag{3}$$

0 otherwise, where $K(k)$ is the complete elliptic integral of the first kind with argument (elliptic modulus) $k \in [0, 1)$. Note that this means that the presence of a homoclinic or heteroclinic orbit implies the presence of a singularity at that value of the function. These two extreme cases are shown in Figure 1. To see the transition from the singular PDF of $\sin x$ to the PDF for $\sin x \sin y$, consider the parameterized family of functions $f_\delta(x, y) = \sin x \sin y + \delta \cos x \cos y$. Figure 2 shows the PDFs of these functions as a function of δ, clearly showing the transition between the two types of behavior. The study of these functions exhibits the dependence on having both unbounded and bounded level sets. Similar dependence has been carefully documented previously in the context of passive scalar transport in which the measure of the unbounded fluid streamlines were shown to play an important role in the ensuing effective large scale mixing.[39–42] In the current context, we will see that the PDF behavior of the transported field will demonstrate subtleties even for pure shear layers with the size of the shear-free zone affecting the width of the distribution.

The PDF considered here is well-defined even for single functions f; an ensemble of fields f is not required to compute $\mathrm{PDF}_f(z)$. Rather, since $\mathrm{PDF}_f(z)$ is the density of a random variable $Y = f(X)$ with X drawn from the uniform distribution on A, the probability density function $\mathrm{PDF}_f(z)$ can be computed as a histogram of spatial samples of f. In what follows, we will be interested in the evolution of fields f that are drawn at the initial time from a measure $\mathrm{d}\mu_{T_0}$. A natural question to ask is whether or not a single PDF computed using (1) bears any relation to a PDF which is averaged over the measure $\mathrm{d}\mu_{T_0}$. Figure 3 shows a comparison between 6 PDFs with different initial conditions and their average. For times up to $t = 100$, these PDFs show a self averaging property. That is, if $T^{(\omega)}(x, y, t)$ is the concentration field at time t with $T^{(\omega)}(x, y, 0) = \omega$ and $PDF^{(\omega)} \equiv \mathrm{PDF}_{T^{(\omega)}(x,y,t)}$, then at least empirically

$$\mathrm{PDF}^{(\omega)} \approx \langle \mathrm{PDF}^{\omega)} \rangle_\omega$$

where $\langle\cdot\rangle_\omega$ represents averaging over the measure $\mathrm{d}\mu_T$. By time $t = 150$, the individual PDFs begin to differ greatly from the average PDF and this self-averaging property ceases to hold. We interpret this as being due to a lack of independent spatial samples at large times (see for example fig. 12(a)). A more thorough study of the time at which self-averaging ceases to hold is not performed here, although it is an interesting question.

III PDF Evolution

A Numerical Simulations

In the following sections we present the results of a family of numerical simulations of the advection-diffusion equation

$$\begin{aligned} \partial_t T + \boldsymbol{u}(\boldsymbol{x}, t) \cdot \nabla T &= \frac{1}{\mathrm{Pe}} \nabla^2 T \\ T(\boldsymbol{x}, t = 0) &= T_0(\boldsymbol{x}) \end{aligned} \tag{4}$$

where T is the *tracer* or *scalar* field and Pe is the *Péclet number*. All times considered here are non-dimensional and should be considered relative to the dynamical timescale L/U where L and U are typical length and velocity scales. All of the flows considered here have $L/U = 2\pi$. The problem domain will be a doubly-periodic square $\boldsymbol{x} \in [0, 2\pi)^2$ with $t \geq 0$. Our numerical method is pseudospectral for the spatial derivatives and the timestepping is via a third-order semi-implicit Runge-Kutta scheme[43] where the diffusive terms are treated implicitly and the (possibly time-dependent) advective terms are treated explicitly. In the following discussion, the fluid velocity will be prescribed, two dimensional, possibly time varying periodic, incompressible flows. All of the simulations below except those that specifically indicate otherwise were run with 1024 Fourier modes in each direction and at $\mathrm{Pe} = 8000$.

Consider a realization over random initial data of the random field $T(x, y, t)$. Formula (1) defines the probability measures we will consider in this article, with scalar field of T consistently determined through the evolution of the passive scalar equation (4). As shown in fig. 3, for moderate time values, averaging over statistical realizations of the initial random field suggests that this system is self averaging in that averaged PDFs do not show strong deviation from individually constructed PDFs. It is an interesting question to consider

the pointwise distribution of tracer, such as might be obtained though fixed mooring stations, which may have different distribution properties than the current construction based on spatial distributions. The particular inhomogeneous deterministic nature of the fluid velocities considered here suggests that the distribution based upon all spatial values of the field is the natural choice for the present study. This is also the type of distribution that is of interest to researchers in this field.[2,3,12,18,27,36,37]

The PDFs shown below were computed as histograms of the numerical solution using 200 equally-spaced bins. The results are not strongly sensitive to the number of bins used. In order to examine the structure of the scalar field for large times, we need to rescale by some factor, since all of our studies are in the case of decaying scalar fields with $\langle T \rangle = 0$, $T \to 0$ pointwise as $t \to \infty$. We choose to rescale by the standard deviation (or equivalently L^2-norm), defining $X = T/\langle T^2 \rangle^{1/2}$.

It has been common in considering advection-diffusion of passive tracers to consider random flows with deterministic initial conditions,[18,34,36,37] or using both random advection and random initial conditions.[5,11,20] In this paper we will consider a different situation with deterministic flow fields but possibly random initial conditions. For our random initial conditions, we will generally use two-dimensional, Gaussian random fields with a specified Fourier spectrum $\hat{\phi}_0(\boldsymbol{k})$. We choose a spectrum that is parameterized by a peak wavenumber k_0[44]

$$\hat{\phi}_0(\boldsymbol{k}) = C \frac{k^7}{(k + 2k_0)^{18}}$$

where $k = |\boldsymbol{k}|$ and the normalization constant C is chosen so that $||\phi||_2 = 1$. The results presented are similar for different choices of the functional form of $\hat{\phi}_0$ so long as they are spectrally broadband. Below we will investigate the effects of varying k_0.

B Planar shear flows

Here we consider unidirectional shear flows with $\boldsymbol{u}(\boldsymbol{x}, t) = (u(y), 0)$ where $u(y)$ is a periodic function of y with period 2π. The evolution of the scalar field and the PDF is shown in figs. 4 and 5 for $u(y) = -\cos y$. (See also the videos available in EPAPS depository.) The spectral evolution is shown in fig. 6. In fig. 5, the evolution of the scalar field is depicted in the left column, while in the right column, we show the corresponding PDF. The field

is initially a Gaussian random field with very small-scale structure ($k_0 = 25$) and a PDF that is initially Gaussian by construction. Over intermediate time-scales, the tails of the PDF become heavier, reaching an approximately exponential shape at $t = 40$. Finally, as the shear and diffusion act to suppress gradients in the region where the shear is largest, the PDF develops a large central core of values near zero and strong tails of anomalously large deviations. In this case, we can interpret the structure of the PDF at long times in terms of the spatial structure of the scalar field, with two large regions of relatively small and homogeneous scalar concentrations and two thinner regions of relatively large fluctuations where the local velocity field is shear-free (i.e. the fluid velocity is extremal). Within the shear-free regions, it is interesting to note the presence of a dominant streamwise length scale (as measured by k_x). Predicting this length scale in relation to the other length scales in the problem is an interesting theoretical question. Work in preparation using WKB analysis will address this issue. It is also interesting to note that the width of the regions of strong fluctuation is dependent on the Péclet number, with smaller regions being associated to larger Péclet numbers.

The evolution of the power spectrum is documented in fig. 6. The dominant trend is the collapse of energy to the largest scales in a non-uniform fashion. By the final time, the majority of the energy is in the largest scales, and it is important to assess the role of the largest "box scale" on the resulting PDFs, which we will discuss next. This collapse has been analyzed by Rhines and Young[45] following the original work of Taylor[46] on shear-enhanced dispersion as well as by Shraiman[47] and many others. Rhines and Young show (among other things) that diffusion in the direction normal to the shear happens at an increased rate relative to diffusion along the shear direction. Spectrally, they show that the y-component of the wave-vector of a single wave increases linearly with time resulting in decay of variance in the downstream direction at a rate proportional to t^3 (which is a familiar result for a linear shear layer). While their analysis explains the distinct decay processes in the sheared and shear-free regions it does not address the impact of this distinction on the scalar PDF distribution as we do here.

We note that for the special case of an initial scalar field which consists of a single mode in the x-direction, the spectral evolution is different. In that case, the overall migration into the origin is not seen, but rather the evolution is confined to a vertical line with k_x fixed by its initial value. Examples of single mode initial scalar fields are considered in detail below in Section IV.

B.1 Box Scale Effects and Resolution

Our simulations are of fluid flow in a doubly-periodic domain which spectrally differs from the doubly-infinite plane in the presence of a lowest possible wavenumber or a longest possible scale. As it is related to the computational box we call this length scale the "box scale". If we are to imagine that our computational box is representative of a small piece of a larger domain, then adding more such adjacent boxes should not change the results. In order to address this we performed a matched set of simulations where the only difference was the size of the computational domain. The computational domain (and the periodicity requirement) were simply doubled in length neither changing the initial scale of the scalar field nor the velocity field. Rather than computationally solving (4) we changed the problem domain to the doubly periodic square $\boldsymbol{x} \in [0, 4\pi)^2$ without changing anything else. In order to keep the resolution of the simulation constant, we double the number of Fourier modes in each direction from 512 to 1024.

Figure 7 depicts a sampling of the PDFs for a simulation involving random initial data with $k_0 = 10$ where the left column depicts the original box and the middle column depicts the doubled spatial domain. There are strong differences between the PDFs from the two simulations especially at later times. This is not surprising, because, as seen in fig. 6, the box scale is clearly important in that it holds much of the energy of the scalar field at later times. The simulation in the larger box contains Fourier modes that are not in the other simulation, in particular those with (original) wavenumber 1/2. By filtering out just these box scale Fourier modes (those with wavenumbers $k_x = 1/2$ or $k_y = 1/2$) we can recover a scalar field more similar to that of the original simulation. Performing this filtering gives the results shown in the right column of fig. 7.

At early ($t = 25$) and late times ($t = 100$), all three PDFs are visually similar. However, the dynamic transition between these two states is quite distinct for the simulations with the differing box sizes. There is an intermediate period of time ($t = 50$) where the simulation in the smaller box (left column) has a PDF with a much more strongly peaked core region than the simulation in the larger box (middle column) along with narrower tails. The filtered PDF in the right column at output time $t = 50$ possesses a core region similar to the smaller box simulation. Further, the subsequent evolution in the filtered field greatly resembles the evolution of the smaller box simulation.

Comparing the filtered fields in the right column with the results in the left column shows that a) shape of the core of the PDF at intermediate times is robust and is not a box-scale artifact and b) the shape of the tails at intermediate times are different with the inclusion of larger length scales. Thus we conclude that the periodic boundary conditions employed in this study do affect the ensuing PDFs but, particularly at long times, features of the generic (boundary condition independent) PDF evolution may be observed in these periodic simulations especially by filtering the long wavelengths. While this present comparison does not fully isolate the effects of the box scale on the long time PDFs, it does suggest that certain features observed in the smaller box scale PDFs are box size independent and generic to the particular transport processes associated with the fluid velocities considered here, namely the depletion of mid-range scalar values builds a peaked core region and, in addition the mid-range fluctuations show PDFs that are concave up in a semi-log plot, reminiscent of a stretched exponential distribution. The detailed effects of the box scale on the evolution of scalar distributions merits further study with larger and larger boxes considered at an attendant increase in computational cost.

To document that these simulations are spatially resolved as well as code independent, we implemented a split step, divided difference based scheme with advection handled second order explicitly, and diffusion handled second order semi-implicitly with time step selected according to CFL criteria. Shown in Figure 8 is the the comparison between the output of the two codes. In Figures 8, 9, and 10, we consider the same parameters as those in Figure 4 except for a different initial realization of the Gaussian random field. In the left panel is the output at time, $t = 22$, for the pseudospectral code with 1024 spatial modes, and in the right panel is output of the split-step scheme, at the same time, with 1000 spatial discretization points. Observe they are nearly identical. Note in these plots, we present the renormalized (by spatial variance) scalar field.

Next, we document that our simulations are well resolved by comparing two cases with different spatial resolutions on a wide range time scales. In Figure 9, we present the short time results of such different resolutions using the split-step scheme. We utilize the same initial data for each spatial resolution by utilizing the same random seed in case. This insures that the modes in a shell of radius smaller than 500 are identical. In the top panel, the evolution of the Fourier spectrum (in modulus) of the raw (non-renormalized) scalar field is shown for the case with 500 spatial nodes, while in the bottom

panel the same is shown with 1000 spatial nodes for short times, $t = 0, 2, 4$.

In Figure 10 we present the same study for longer times $t = 10, 20, 30$. Here, since the fields decay so rapidly to zero, to make the comparison we renormalize the scalar field before computing the Fourier spectrum. Again, observe that the spectral evolution is nearly indistinguishable, with all observable spectral energy confined within a shell of modes of radius approximately 150.

B.2 Other Shear Profiles

To verify our interpretation of the PDF in relation to the spatial structure of the scalar field, we also investigated two other nonlinear, periodic shears:

$$u_1(y) = 2\left(\frac{1-\cos y}{2}\right)^5 - 1 \text{ and}$$
$$u_2(y) = C\left(\sin(y) - \frac{1}{9}\sin(3y) + \cdots + \frac{1}{169}\sin(13y)\right)$$

which are shown in the first column of fig. 11. Velocity u_2 is given by the first seven terms in the Fourier series expansion of a triangle wave and C is chosen so that it has maximum value 1. The shear flow u_1 has a much larger region of small velocity gradients (shear-free) than does $-\cos y$ and conversely u_2 has a smaller shear-free region. The results of these simulations are summarized in fig. 11. Recall that we explained the heavy tails of the scalar distribution in fig. 11(a) as being due to the large fluctuations that persist in the shear-free regions while the core of the distribution is determined by the small fluctuations in the strongly sheared regions.

In fig. 11(b), we see the field and PDF at time $t = 150$ for the velocity profile with larger shear-free regions. The spatial structure of the scalar field is as we would suspect, with large fluctuations still present in the (large) shear-free regions and homogeneous, small scalar values in the strongly sheared regions. Looking at the PDFs, in this case the core region of the PDF is smaller relative to the tails—indeed the core is almost non-existent. The tails seems to be less broad than those seen in fig. 11(a) but this is due to rescaling of the primitive variable T by $\langle T^2\rangle^{1/2}$ where the areal average in this case is larger due to the narrower shear zone On the other hand, in fig. 11(c) we see the results for the velocity field u_2 with a much smaller shear-free region. Here the core region is much larger as we expect, because less of

the domain contains scalar values far from the mean. Again, the tails look larger than for the shears with larger shear-free regions but this is because of the normalization used. The width of the tails is only measured relative to the root mean square (RMS) value of the particular field and for different velocity fields the RMS scalar value can vary widely. Thus we confirm that the core of the PDF is set by the size of the strongly sheared region while the tails are determined by global properties of the flow.

C Parametric initial data dependence

Having explored the physical mechanisms in shear flows that explain the structure of the PDFs for a particular value of k_0 we now turn our attention to the parametric dependence of these PDFs on the dominant length scale of the initial data. The appearance of heavy tails depends on the scale of the initial data relative to the length scale determined by the velocity field. In figs. 12, the fields and PDFs are shown for three different initial scales at time $t = 150$. For $k_0 = 10$, the largest scale initial data, we do not see heavy tails and in physical space there does not appear to be a distinction between the shear-free and highly sheared regions. Conversely for $k_0 = 50$ and $k_0 = 63$ we see heavy tailed distributions and a clear distinction between the two dynamical regions. The length scale of variation in the initial data must be sufficiently small that significant variation is present in the shear-free region. If not, then the longitudinal structures in the sheared regions (which are predicted by Rhines and Young[45]) are of comparable amplitude with the fluctuations in the shear-free region and thus no core/tail distinction appears in the PDF. Once the initial wavenumber exceeds a critical value, heavy-tailed PDFs appear and are insensitive to the initial scale. We mention that these PDFs are transient in time and that, for different velocity fields, heavy tailed distributions do not appear at any length scale. For example, if we replace the fluid velocity by $u(y) = u_2(3y)$ we do not see heavy-tailed distributions for any of the length scales that we can study at this resolution.

In fig. 12 and throughout much of the paper we present results comparing the state of the scalar field at a fixed time for different parameter values. In order to document that the differences shown at the same time are not artifacts of the varying decay timescales for different length scales, we show in fig. 13 the complete PDF evolution for $k_0 = 10, 25, 50$, and 63. As seen there, the PDF behavior is qualitatively different for the different length-scales, not merely a rescaling of time by some unknown factor. In particular

there is a lack of a strongly peaked core of the PDF with $k_0 = 10$ and a clear presence for $k_0 = 50$ and $k_0 = 63$. Also, there is a universal emergence of an exponential PDF for $k_0 = 25, 50, 63$ over the same time period $t = 40, \ldots, 70$ which precludes the possibility that the behavior of the PDF for these initial length scales is simply a temporal rescaling of the behavior for other initial length scales. We also note that part (d) in fig. 12 does not show intermediate time behavior that resembles that of part (a). Thus the evolution for $k_0 = 63$ will not resemble that for $k_0 = 10$ under any possible rescaling of time.

Another feature of the scalar field evolution in these nonlinear shear flows are ripples in the region of the flow that is smoothed out by the large shear. The ripples can be seen as a light striation in the largely gray regions of fig. 11 and clearly in fig. 12(a). The amplitude of these structures are stationary in time when rescaled by the scalar standard deviation (see fig. 14). The amplitude also shows sensitivity to the length scale of the initial data, with the amplitude of the ripples being larger for smaller values of k_0. This scale dependence of the ripples provides an explanation for the scale dependence of the PDFs (see figs. 14(c) and 14(d)) if we think of the sheared region where the ripples appear as being responsible for the core of the PDF and the unsheared regions as being responsible for the tails. Then, if the amplitude in the rippled region is closer to that of the unsheared regions, the *width* of the core of the PDF is larger as seen in fig. 14. The temporal stationarity of the spatial structure is suggestive of the 'strange eigenmode' approach to scalar mixing[18,36] (see Section IV).

As a final feature of interest, we investigate the time evolution of the moments of the scalar field $\langle |T|^n \rangle$. The decay rate of the variance (second moment) has been studied at length in the context of turbulent flow.[5–7,11,15,20–23,31–33] If the scalar evolution is self-similar (that is, stationary for an appropriately rescaled variable, in this case X) then the decay of the moments will be prescribed: if $\langle |T|^n \rangle \sim \exp^{-\alpha_n t}$ with α_n growing linearly in n. As seen in fig. 5, the PDF for the scalar in our shear flow approaches an invariant form for long times, so we should expect to see self-similar behavior in the moments. Figure 15(a) clearly shows exponential decay for the moments after $t \approx 100$. This is exactly the time period over which the scalar field shown in fig. 14(a) has stationary spatial structure. In order to verify that the moments decay as expected, we least-squares fit a line to the logarithm of the moments over the time period when they show exponential decay and estimate α_n as the slope of that line. We see that the moment decay rates grow linearly with n as expected with (fig. 15(b)). Self-similar behavior also appears for other

values of k_0, except that the time at which the evolution becomes self-similar varies.

D Cellular flows

In order to consider a flow with a more fully two-dimensional structure, we consider the flow induced by the streamfunction

$$\psi(x,y,t) = \sin(x - \epsilon c_1(t)) \sin(y - \epsilon c_2(t)) \qquad (5)$$
$$c_1(t) = \cos(\omega t), \quad c_2(t) = \sin(\omega t)$$

for fixed parameters ϵ and ω. If $\epsilon > 0$ and $\omega > 0$ then this flow has chaotic trajectories and positive Lyapunov exponents in parts of the domain. While chaotic advection is present in this flow, it is not a necessary condition for heavy-tailed scalar PDFs. Figure 16 shows the scalar evolution in the case where $\epsilon = 0$. (See also the video available in EPAPS depository.) The pattern is very similar to that seen in the previous section for shear flows: the initially Gaussian PDF has increasingly heavy tails, passing through exponential until finally having both strong tails as well as a well-defined core. Over the duration of this simulation to $t = 100$, the PDF never achieves a stationary state.

With $\epsilon > 0$, the particle trajectories are chaotic but this appears not to have any dramatic effects on the structure of the PDFs. Figure 17 shows the evolution with $k_0 = 63$, $\omega = 10$ and $\epsilon = 0.1$. The results are very similar to those in fig. 16 with slightly less heavy tails. These results are also mostly insensitive to changes in ω (fig. 18(a)) and k_0 (fig. 18(b)) with a slight exception for $k_0 = 10$ where we see a strong distinction between the core and tails as in fig. 16. This cellular flow does show a Péclet number dependence, with very low Péclet numbers having a nearly Gaussian PDF for all times (as is expected for $\mathrm{Pe} \to 0$) and higher Péclet numbers having more heavy-tailed, non-Gaussian PDFs as shown in fig. 19. The PDF results for time-independent cellular flows (with $\epsilon = 0$) are very similar to those shown in fig. 18(b).

We can attempt to provide an explanation for the PDF structure similar to that given for shear flows in section B. Figures 20 and 21 show the detailed structure of the evolution of the scalar field in the case of $\epsilon = 0.1$ and $\omega = 2$. (See also the videos available in EPAPS depository.) The decomposition of the domain into separate regions of distinct behavior is not appropriate as it

was before. Both the centers of the cells and the boundary regions are filled with filamentary structures that appear in fig. 21 as deep canyons and high ridges. The steepness of these filamentary structures is the source of the non-Gaussianity seen in the PDFs for these cellular flows. As the steepness of the 'canyon walls' increases, the area where the scalar has values of intermediate size is lessened. This is reflected in the PDF as increasingly heavy tails and smaller probability for values in between the very large and very small. The evolution of the PDFs shown for these cell flows then is explained by the increasing dominance of filamentary structures that have large probabilities of anomalously large values of the scalar. This suggestion that the degree to which filamentary structures dominate the flow determines the PDF also explains the presence of heavy tails only at large Péclet numbers. For lower Péclet numbers, the stronger effect of diffusion relative to advection prevents the formation of steep filaments and thus the formation of heavy tailed PDFs. The limiting behavior for large Péclet numbers is expected to be sensitive, because for $1/\mathrm{Pe} = 0$, the PDF is preserved exactly under the action of an incompressible fluid flow and thus should remain Gaussian for all time if it is initially Gaussian. It is not known what the PDF structure is in the limit of large Péclet numbers.

Looking at the long-time moment decay for this time-dependent cellular flow in fig. 22(a), we can see that this flow never settles down into a self-similar eigenmode. The moment decay is never exponential with a constant rate. It is not possible to consistently fit a single exponential to even a sub-interval of the data as shown in fig. 22(b). If we try to fit an exponential decay to the data for $t \in [t_0, 900]$ then the fitted decay rate depends strongly on the choice of t_0. In the case of time-independent cellular flow (when $\epsilon = 0$) we do see self-similarity analogous to that seen in section C. The time-dependent case presented here is in contrast to both the self-similar[18,34,36] and the non-self-similar[31,32] theories of passive scalar variance decay. The flow considered here does not satisfy the length-scale assumptions made in either case: the length scale for scalar variation approaches the length scale of the flow, so as to violate the scale assumption of Balkovsky and Fouxon,[32] and the flow considered here is not globally mixing in the sense considered by Fereday and Haynes.[34] Sukhatme and Pierrehumbert[36] analyze this situation for random flows with a range of Lyapunov exponents, but we are not aware of a theoretical analysis of the decay of passive scalars in such partially mixing flows at length scales comparable with those present in the flow.

Haller and Liu[28] have shown that a finite-dimensional inertial manifold

exists for this advection-diffusion problem and thus the long-time decay of the scalar field should be governed by the structure of the slowest-decaying mode in that manifold, provided that the components of the field that lie outside of the inertial manifold decay fast enough. The absence of obvious exponential decay of the moments in this case of time-periodic perturbed cellular flows does not contradict their theory, rather it suggests that the evolution over this intermediate time period is governed by a large number of eigenmodes that all remain present over the length of the simulation.

IV Coherent Initial Data for Shear Flows

In an effort to understand the dynamical processes affecting the scalar PDF, we consider the simplified case of initial data that is spectrally single mode

$$T(x, y, t = 0) = \sin(k_0 x) \sin(k_0 y)$$

in the nonlinear shear flow with $u(y) = -\cos y$. The scalar evolution is shown in fig. 23 and the moment evolution in fig. 24. The scalar evolution proceeds with a dramatic reduction of variation in the sheared regions and preservation of the streamwise structure in the two bands where the shear is not present. Eventually, the sheared regions become completely flat and the bands of variation that remain reach a stationary configuration consisting of two counter-flowing bands. The PDF is initially as shown in fig. 1 for the function $\sin x \sin y$. Large tails develop, reflecting the presence of regions of large variability along with regions of almost no variability. Since $X = T/\langle T^2 \rangle^{1/2}$, the presence of large regions with $T \approx 0$ reduces the standard deviation and so increases the maximum value attained by X inside the shear-free regions.

The self-similar regime is achieved much more rapidly for these initial conditions than it was for the spectrally broadband initial conditions discussed in section B. In fact, past $t = 50$ the PDF is essentially stationary for the remainder of the simulation. Qualitatively, the evolution is invariant with changes in the free parameters k_0 and Pe, with the onset of self-similarity coming earlier for larger values of k_0 and smaller values of Pe. The width of the bands of variability is dependent on Péclet number as it was for the random initial conditions.

The rapid adjustment to self-similarity makes these single mode initial conditions ideal for studying the dependences of the decay rates α_n on the

parameters. Similarly to section B, fitting exponential curves to the self-similar regime variance decay rate gives estimates for α_2. Because the PDFs are self-similar, α_n is a linear function of n and we will only consider the parametric effects on α_2. The results of these estimated parameters are shown in fig. 25 for changes in k_0 and Pe. We observe a linear dependence of the decay rate on $\kappa = 1/\mathrm{Pe}$ and a nonlinear dependence on k_0. For non-chaotic flows, this is the expected behavior of α_2 for small κ while for chaotic flows the limit of α_2 as $\kappa \to 0$ remains unresolved.[35,48]

The decay rates α_2 computed here are just the square of the real part of the least negative eigenvalue of the eigenproblem

$$\sigma\hat{T}(y) + ik_0u(y)\hat{T} = \kappa\left(-k_0^2T + \partial_y^2T\right) \tag{6}$$

$$\hat{T}(y) = \hat{T}(y + 2\pi) \tag{7}$$

which comes from (4) by making the separation of variables ansatz $T(x, y, t) = e^{\sigma t}e^{-ik_0x}\hat{T}(y)$ inspired by the form of the numerical solutions seen above. This is just Hill's equation[49] with a complex potential. The periodic solutions of this complex Hill's equation should give the decay rate of T explicitly.

In the case of the cellular flow with coherent initial data, the eigenvalue problem involves the full two-dimensional Laplacian and the analysis becomes more involved. We observe in fig. 26 that the PDF does achieve a self-similar form much like that seen in the case of shear flow. This PDF corresponds to the eigenmode of the two-dimensional eigenvalue problem whose eigenvalue is the slowest decay rate. The detailed analysis of these eigenvalue problems is beyond the scope of the present paper and is the subject of a forthcoming study.

V Conclusion

We have shown above the results of simulations of passive scalar advection diffusion in a series of simple fluid flows. Previous work in this topic has focused on random flow, often in the context of lattice maps[18,34,36] or random shear flows.[5–7,11,15] Here we have focused on trying to understand in basic fluid flows the physical processes that dynamically determine the structure of the scalar probability distribution functions (PDFs). We began by looking at the PDF of known functions, to emphasize what structures could be identified by looking at these distributions. We then investigated the evolution of the

scalar PDFs in the case of nonlinear shear flows. We found that the observed PDFs could be explained by decomposing the flow into regions of shear and non-shear. Diffusion acts preferentially in the sheared regions and thus the scalar values in those regions relax to their equilibrium value faster than in the regions where there is no shear. The shear region appears in the PDFs as a large core region of values near zero. Conversely, in the non-sheared regions we see persistent large variations in scalar values which appear as long tails in the scalar PDF. This approach to PDFs is confirmed by experiments using different nonlinear shears with both larger and smaller non-shear regions. Varying the length scales of the initial perturbation field leads to evolutions that follow the same general pattern as that described above but vary in the details. In particular the initial data must be sufficiently small scale to observe heavy tailed PDFs. The sheared regions develop stationary ripples at long times and the size of these ripples determines the shape of the PDF. This stationarity of regions of the flow suggests that what we are seeing is a self-similar eigenmode solution of the passive scalar problem. Analysis of the decay of higher order moments, in particular the linear dependence of the decay rate on the moment number, confirms that the decay is self-similar at long times. When nonlinear shear flows are replaced by fully two-dimensional spatially dependent flows and periodic time dependence is introduced, we do not see exponential decay of the moments. Over a very long simulation (fig. 22) we do not see stationarity in the PDFs nor in the associated moments. This is in distinction to random flows with small-scale initial data as previously studied in the literature.[5–7,11,15,18,31,32,34,36,50]

The evolution of the PDFs for cellular flows we have examined, both constant and time-dependent, is qualitatively similar to that seen for shear flows with the development of heavy tails at large times. For the time dependent flows we have considered, their chaotic nature does not appear to be a factor in the development of these heavy tails, as might have been expected from their appearance in pure shear flows.

As a first step toward a theoretical explanation of the PDFs evolution we have observed, we examined the case of single mode initial data. For coherent initial data, the evolution of the PDF is simple and very rapidly exhibits self-similar decay. This rapid adjustment to a self-similar form allows the easy investigation of the decay rate α_2 on the parameters of the problem. We see a linear relationship between α_2 and $\kappa = 1/\mathrm{Pe}$ and a nonlinear relationship between α_2 and k_0. In a forthcoming paper we will study these decay rates through the analysis of periodic solutions of a complex Hill's Equation.

There is much work still to be done in the evolution of scalar PDFs for spatially inhomogeneous flows. A rigorous analysis of the eigenfunctions of the advection-diffusion problem appears possible and can explain the asymptotic scalings of the moment decay rates for the problem of simple shear. Due to the size of these simulations, it can be difficult to generate enough data, particularly in situations, such as long times, where ensemble calculations might be necessary. Larger families of simulations could begin to answer questions about the very long time behavior of these systems as well as their relationship to the eigenmode theory. Time-windowing might also be used to give the illusion of more data, although in a transient evolution such as this, windowing can be problematic. Finally this work might be expanded by simulations of geophysically relevant flows similar to those present in the atmosphere and ocean where observations have been made.

VI Acknowledgments

We profited from discussions with Chris Jones on this project. The authors also wish to thank the final reviewer whose suggestions helped to better crystallize the loose connection between the PDF under study here and the single point field statistics. RMM and NM-B were partially supported by a National Science Foundation Collaborations in Mathematical Geosciences (CMG) Award, NSF ATM-0327906. RMM was also partially supported by NSF DMS-030868. RC was partially supported by NSF DMS-0104329 and DMS-0509423. Computational work was supported by NSF DMS-MRI 0116625 and DMS-SCREMS 0422417.

References

[1] B. Castaing, G. Gunaratne, F. Heslot, L. Kaadanoff, A. Libchaber, S. Thomae, X.-Z. Wu, S. Zaleski, and G. Zanetti, "Scaling of hard thermal turbulence in Rayleigh-Bénard convection," J. Fluid Mech., **204**, 1 (1989).

[2] L. Sparling and J. Bacmeister, "Scale dependence of trace microstructure: Pdfs, intermittency and the dissipation scale," Geophys. Res. Lett, **28**, 2823 (2001).

[3] R. Ferrari and D. L. Rudnick, "Thermohaline variability in the upper ocean," J. Geophys. Res., **105**, 16857 (2000).

[4] V. Yakhot, S. Orszag, S. Balachandar, E. Jackson, Z.-S. She, and L. Sirovich, "phenomenological theory of probability distributions in turbulence," J. Sci. Comp., **5**, 199 (1990).

[5] J. Bronski and R. McLaughlin, "passive scalar intermittency and the ground state of schrödinger operators," Phys. Fluids, **9**, 181 (1997).

[6] J. Bronski and R. McLaughlin, "Rigorous estimates of the probability distribution function for the random linear shear model," J. Stat. Phys., **1998**, 897 (2000).

[7] J. C. Bronski and R. M. McLaughlin, "The problem of moments and the Majda model for the random linear shear model," Physics Letters, **265**, 257 (2000).

[8] R. H. Kraichnan, "Small-scale stucture of a scalar field convected by turbulence," Phys. Fluids, **11**, 945 (1968).

[9] M. Chertkov, "Instanton for random advection," Phys. Rev. E, **55**, 2722 (1997).

[10] Z. She and S. Orszag, "Physical model of intermittency in turbulence: Inertial range non-gaussian statistics," Phys. Rev. Lett., **66**, 1701 (1991).

[11] A. Majda, "The random uniform shear layer: an explicit example of turbulent diffusion with broad tail probability distributions," Phys. Fluids A, **5**, 1963 (1993).

[12] Y. G. Sinai and V. Yakhot, "Limiting probability distributions of a passive scalar in a random velocity field," Phys. Rev. Lett., **63**, 1962 (1989).

[13] B. Shraiman and E. Siggia, "Lagrangian path integrals and fluctuations in random flow," Phys. Rev. E, **49**, 2912 (1994).

[14] J. C. Bronski, "Asymptotics of Karhunen-Loeve eigenvalues and tight constants for probability distributions of passive scalar transport," Comm. Math. Phys., **238**, 563 (2003).

[15] E. Vanden-Eijnden, "Con-Gaussian invariant measures for the Majda model of decaying turbulent transport," Comm Pure Appl. Math., **54**, 1146 (2001).

[16] E. Balkovsky and A. Fouxon, "Two complimentary descriptions of intermitency," Phys. Rev. E, **57**, R1231 (1998).

[17] M. Holzer and E. Siggia, "Skewed, exponential pressure distributions from gaussian velocities," Phys. Fluids A, **5** (1993).

[18] R. T. Pierrehumbert, "Lattice models of advection-diffusion," Chaos, **10**, 61 (2000).

[19] A. Bourlioux and A. J. Majda, "Elementary models with probability distribution function intermittency for passive scalars with a mean gradient," Phys. Fluids, **13**, 881 (2002).

[20] R. McLaughlin and A. Majda, "An explicit example with non-Gaussian probability distribution for nontrivial scalar mean and fluctuation," Phys. Fluids, **8**, 536 (1996).

[21] M. Chertkov and V. Lebedev, "Decay of scalar turbulence revisited," Phys. Rev. Lett., **90**, 034501 (2003).

[22] V. Lebedev and K. Turitsyn, "Passive scalar evolution in peripheral regions," Phys. Rev. E, **69**, 036301 (2004).

[23] S. Boatto and R. Pierrehumbert, "Dynamics of a passive tracer in a velocity field of four identical point vortices," J. Fluid Mech., **394**, 137 (1999).

[24] H. Aref, "Stirring by chaotic advection," J. Fluid Mech., **143**, 1 (1984).

[25] J. Ottino, "Mixing, chaotic advection and turbulence," Ann. Rev. Fluid Mech., **22**, 207 (1990).

[26] E. H. D. Rothstein and J. Gollub, "Persistent patterns in transient chaotic fluid mixing," Nature, **401**, 770 (1999).

[27] R. Pierrehumbert, "Tracer microstructure in the large-eddy dominated regime," Chaos Solitons Fractals, **4**, 1111 (1994).

[28] W. Liu and G. Haller, "Strange eigenmodes and decay of variance in the mixing of diffusive tracers," Physica D, **188**, 1 (2003).

[29] J.-L. Thiffeault, "The strange eigenmode in lagrangian coordinates," Chaos, **14**, 531 (2004).

[30] J. T.M. Antonsen, Z. Fan, E. Ott, and E. Garcia-Lopez, "The role of chaotic orbits in the determination of power spectra," Phys. Fluids, **8**, 3094 (1996).

[31] D. Son, "Turbulent decay of a passive scalar in the batchelor limit: Exact results from a quantum mechanical approach," Phys. Rev. E, **59**, R3811 (1999).

[32] E. Balkovsky and A. Fouxon, "Universal long-time properties of lagrangian statistics in the Batchelor regime and their application to the passive scalar problem," Phys. Rev. E, **60**, 4164 (1999).

[33] D. Fereday, P. Haynes, A. Wonhas, and J. Vasilicos, "Sacalar variance decay in chaotic advection and Batchelor-regime turbulence," Phys. Rev. E, **65**, 035301 (2002).

[34] D. Fereday and P. Haynes, "Scalar decay in two-dimensional chaotic advection and Batchelor-regime trubulence," Phys. Fluids, **16**, 4359 (2004).

[35] P. Haynes and J. Vanneste, "What controls the decay of passive scalars in smooth flows?" Phys. Fluids, **17**, 097103 (2005).

[36] J. Sukhatme and R. T. Pierrehumbert, "Decay of passive scalars under the action of single scale smooth velocity fields in bounded two-dimensional domains: From non-self-similar probability distribution functions to self-similar eigenmodes," Phys. Rev. E, **66**, 056302 (2004).

[37] J. Sukhatme, "Probability density functions of decaying passive scalars in periodic domains: An application of sinai-yakhot theory," Phys. Rev. E, **69**, 056302 (2004).

[38] R. Camassa and S. Wiggins, "Chaotic advecion in a rayleigh-bénard flow," Phys. Rev. A, **43**, 774 (1991).

[39] P. McCarty and W. Hosthemke, "Efective diffusion coefficient for steady two-dimensional convective flow," Phys. Rev. A, **37**, 2112 (1988).

[40] A. Majda and R. McLaughlin, "The effect of mean flows on enhanced diffusivity in transport by incompressible periodic velocity-fields," Studies in Applied Mathematics, **89**, 245 (1993).

[41] A. Fannjiang and G. Papanicolaou, "Convection enhanced diffusion for periodic flows," SIAM J. Appl. Math., **54**, 333 (1994).

[42] R. McLaughlin, "Numerical averaging and fast homogenization," J. Stat. Phys., **90**, 597 (1998).

[43] P. R. Spalart, R. D. Moser, and M. M. Rogers, "Spectral methods for the Navier-Stokes equations with one infinite and two periodic directions," J. Comput. Phys., **96**, 297 (1991).

[44] J. C. McWilliams, "The vortices of two-dimensional turbulence," J. Fluid Mech., **219**, 261 (1990).

[45] P. Rhines and W. Young, "How rapidly is a passive scalar mixed within closed streamlines?" J. Fluid Mech., **133**, 133 (1983).

[46] G. Taylor, "Dispersion of soluble matter in solvent flowing slowly through a tube," Proc. Roy. Soc. London, **A293**, 310 (1953).

[47] B. Shraiman, "Diffusive transport in a rayleigh-benard convection-cell," Phys. Rev. A, **36**, 261 (1987).

[48] Y. Tsang, T. Antonsen, and E. Ott, "Exponential decay of chaotically advected passive scalars in the zero diffusivity limit," Phys. Rev. E, **71**, 0666301 (2005).

[49] W. Magnus and S. Winkler, *Hill's Equation*, Wiley Interscience, New York (1966).

[50] A. Majda and P. Kramer, "Simplified models for turbulent diffusion: theory, numerical modelling, and physical phenomena," Physics Reports, **314**, 237 (1999).

List of Figures

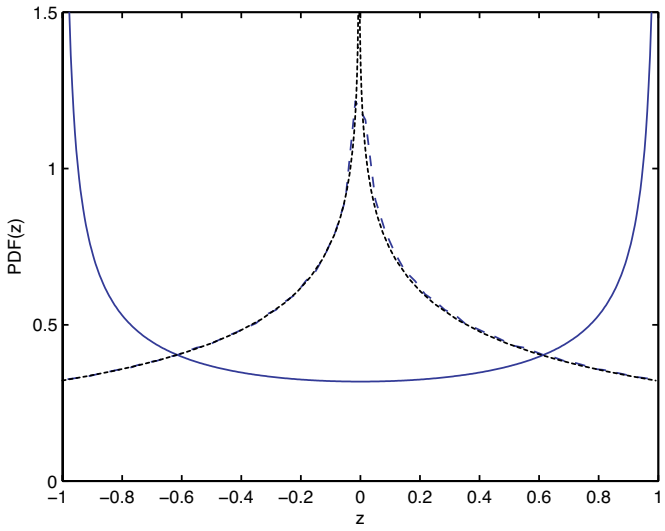

Figure 1, Camassa, Physics of Fluids

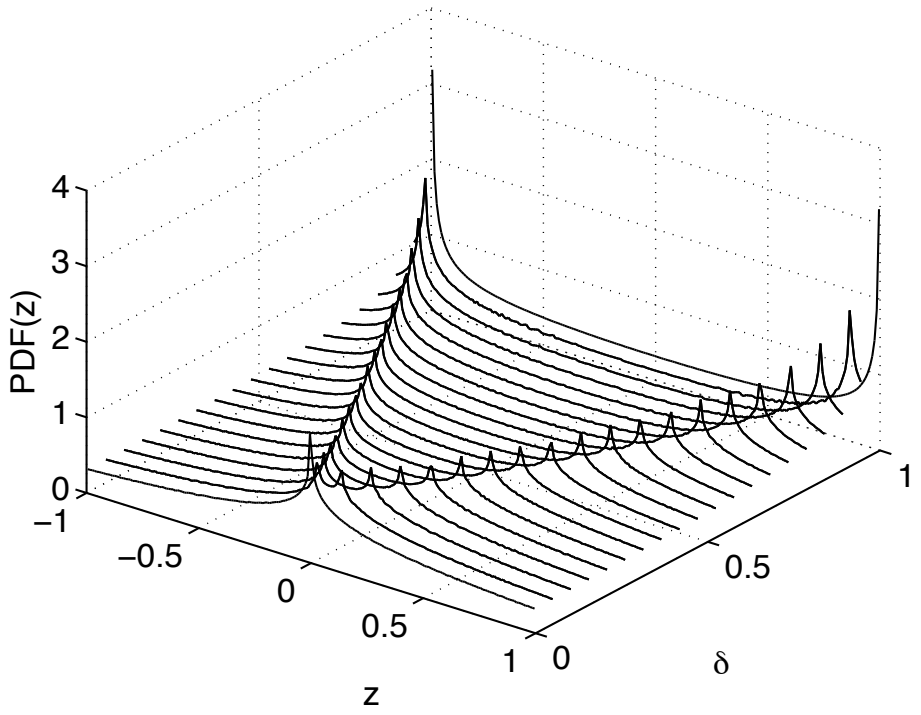

Figure 2, Camassa, Physics of Fluids

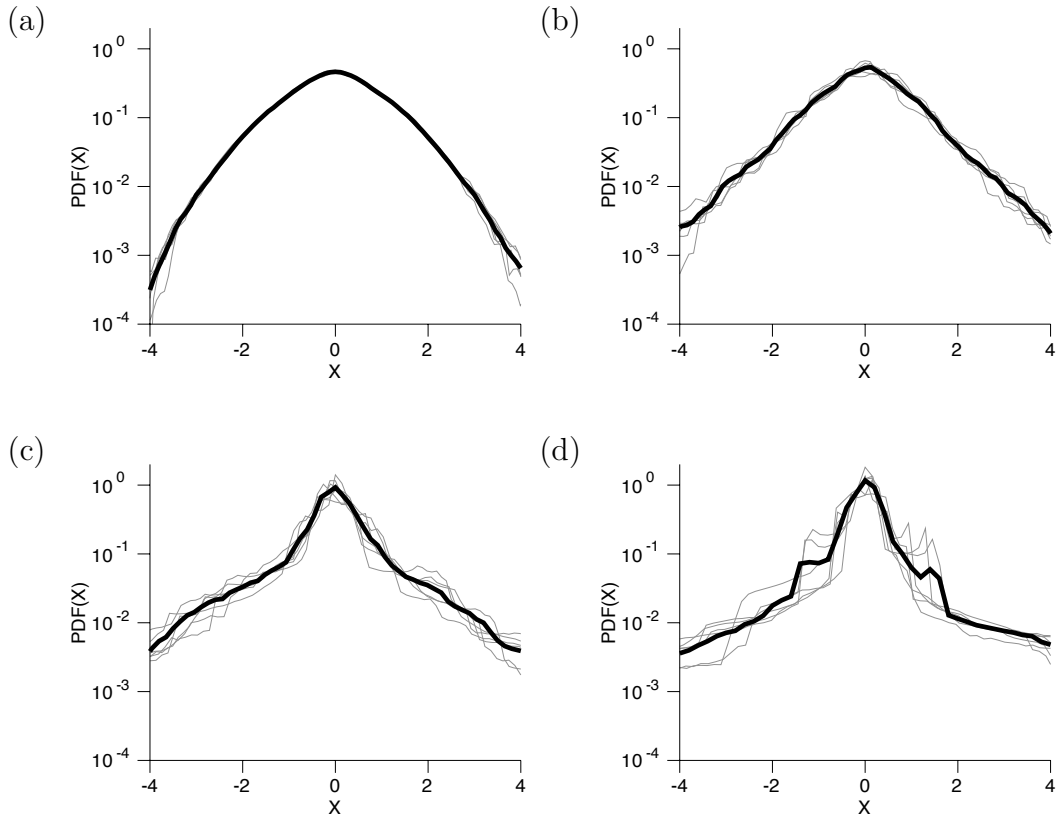

Figure 3, Camassa, Physics of Fluids

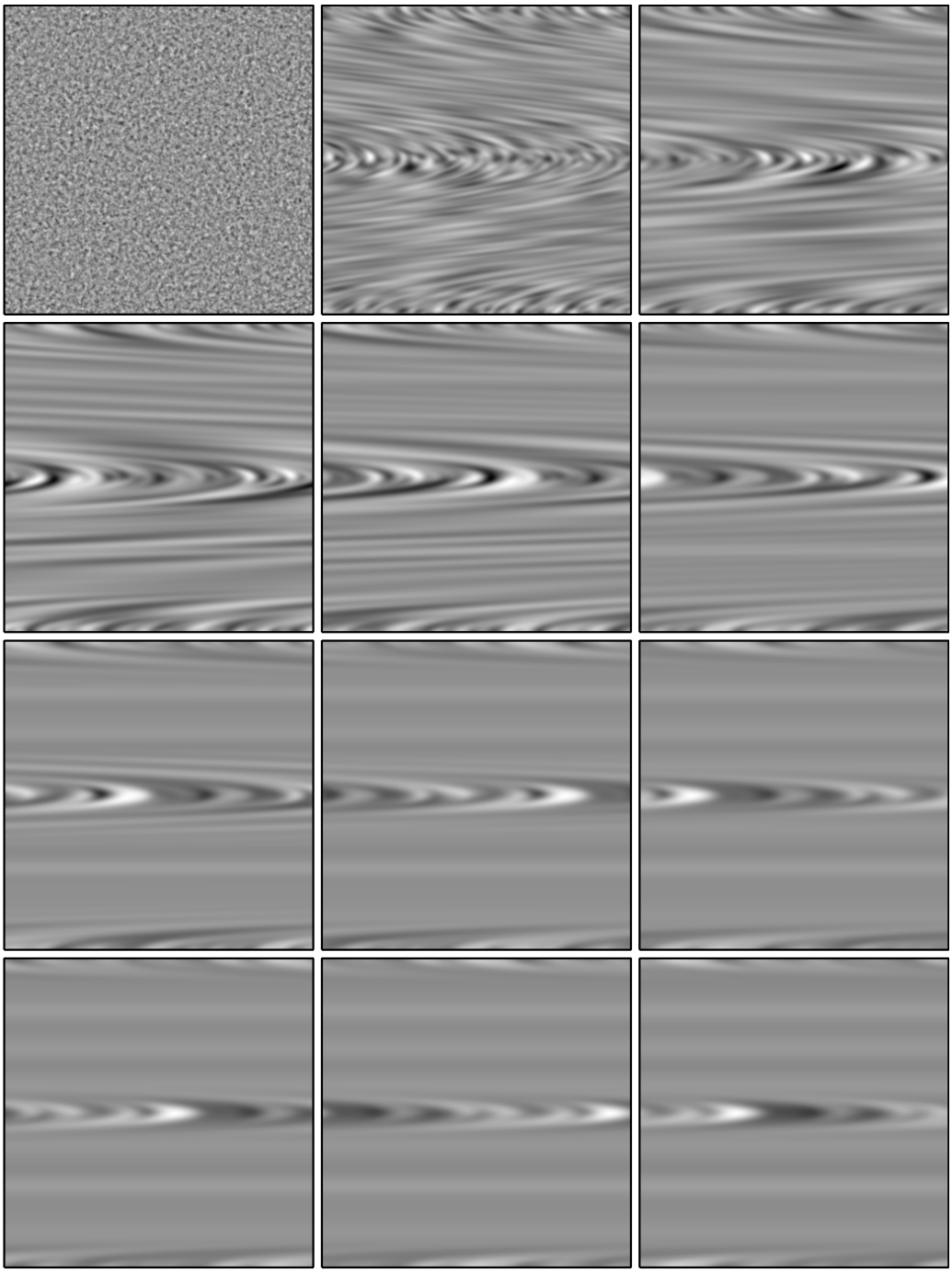

Figure 4, Camassa, Physics of Fluids

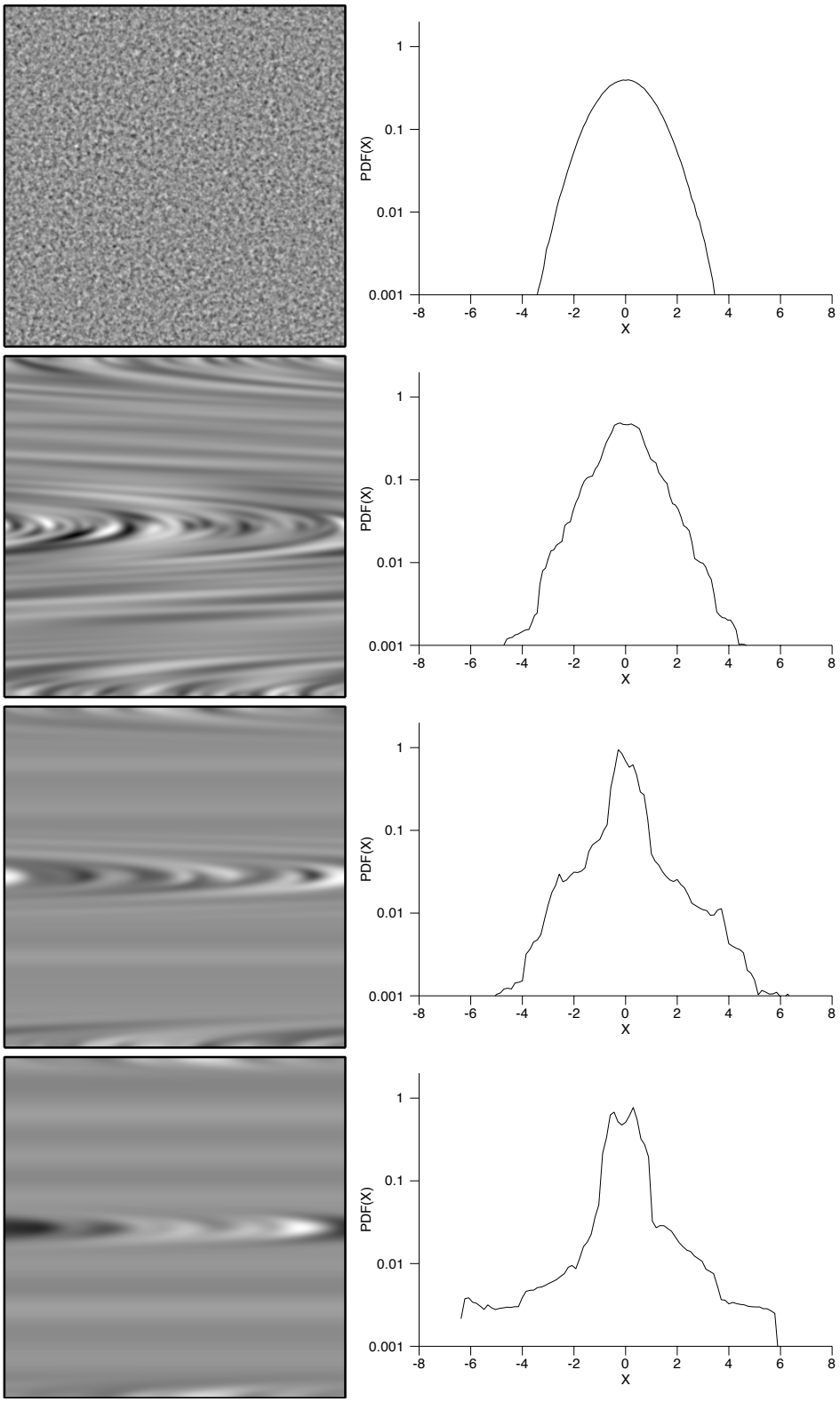

Figure 5, Camassa, Physics of Fluids

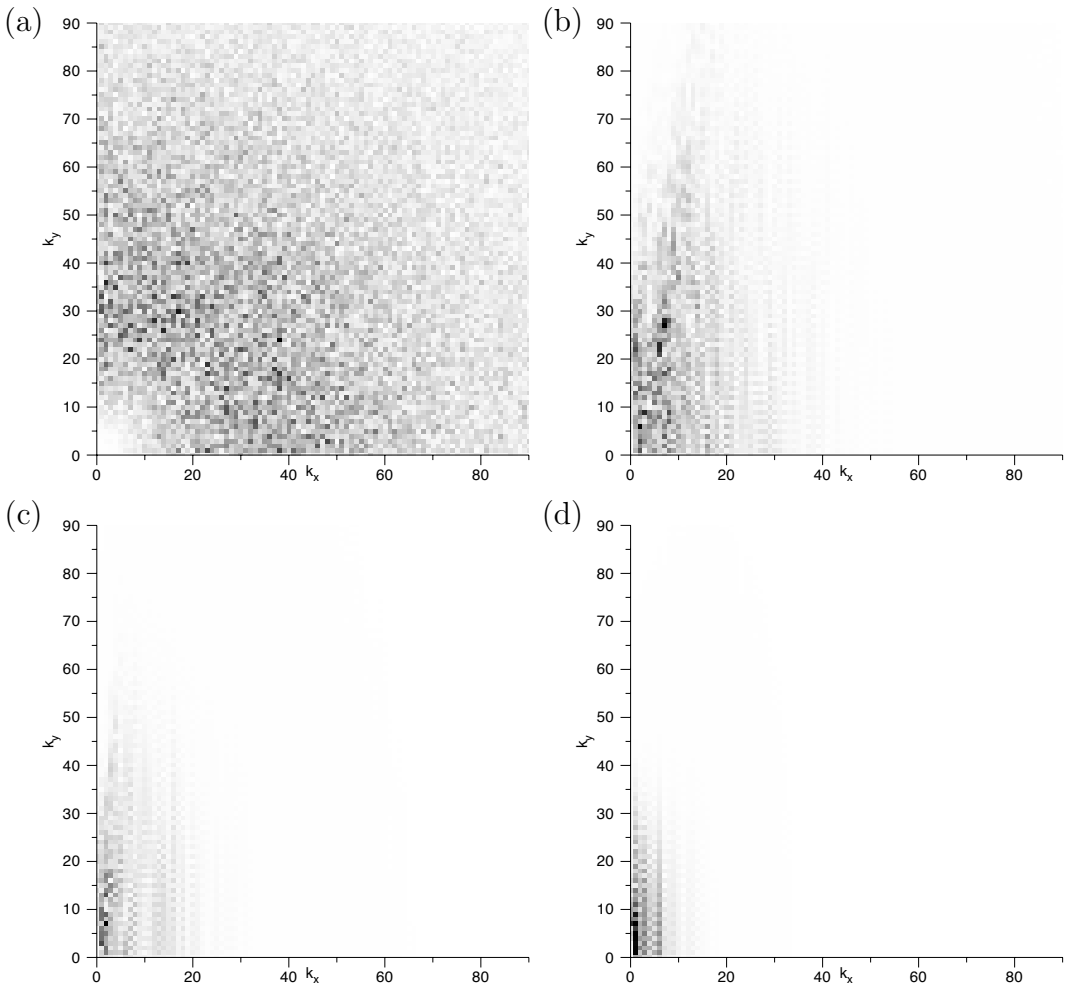

Figure 6, Camassa, Physics of Fluids

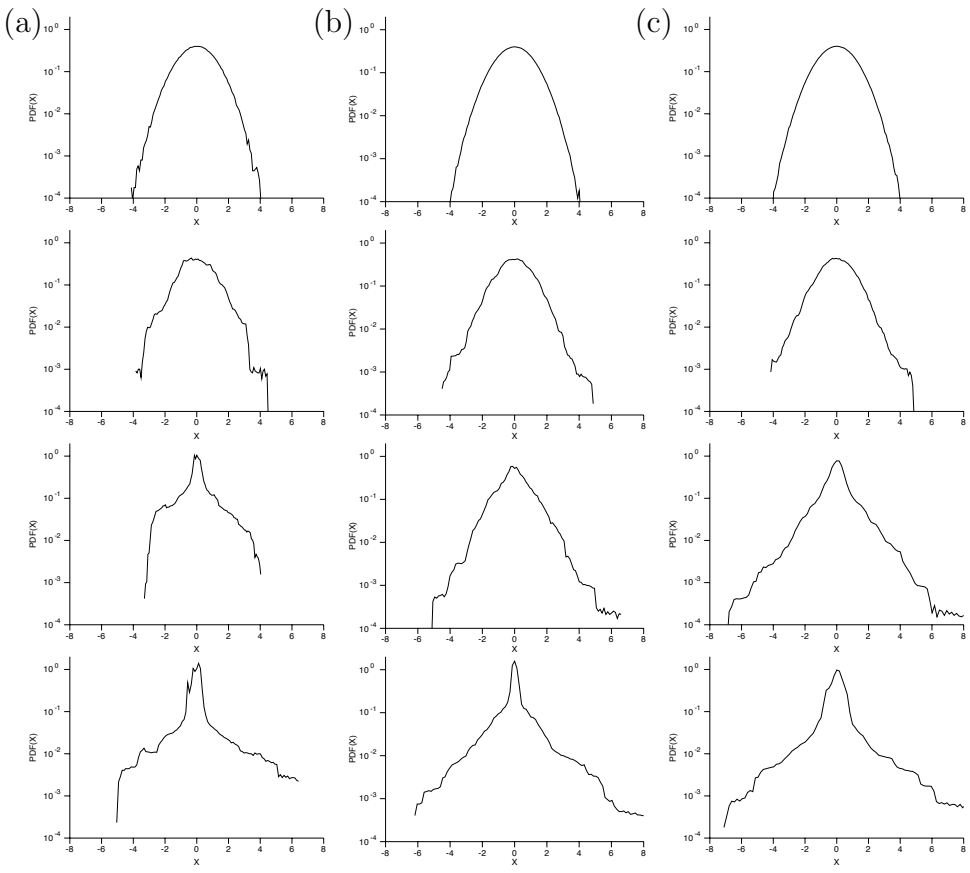

Figure 7, Camassa, Physics of Fluids

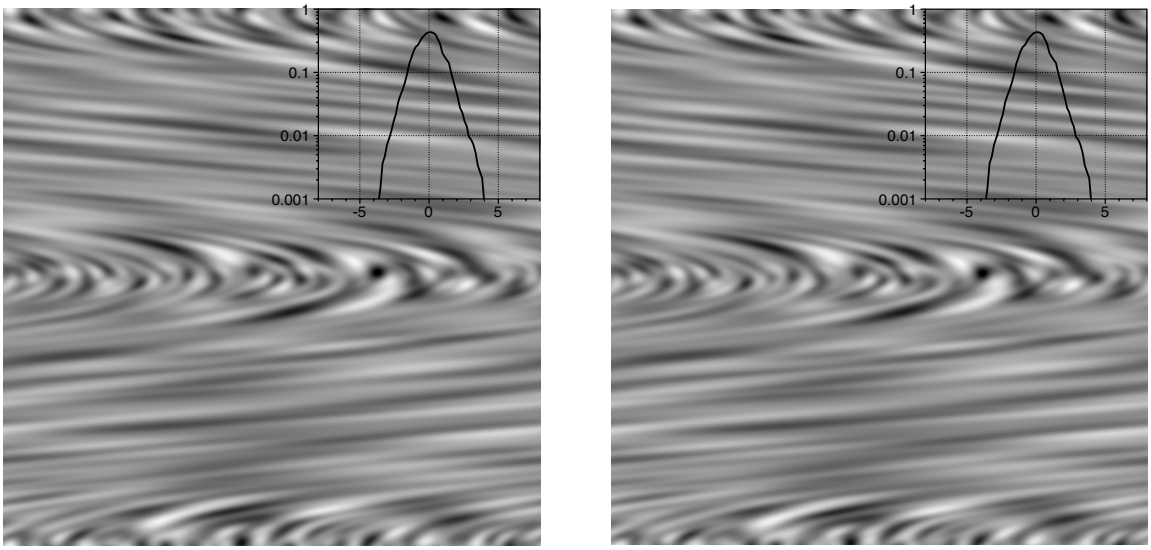

Figure 8, Camassa, Physics of Fluids

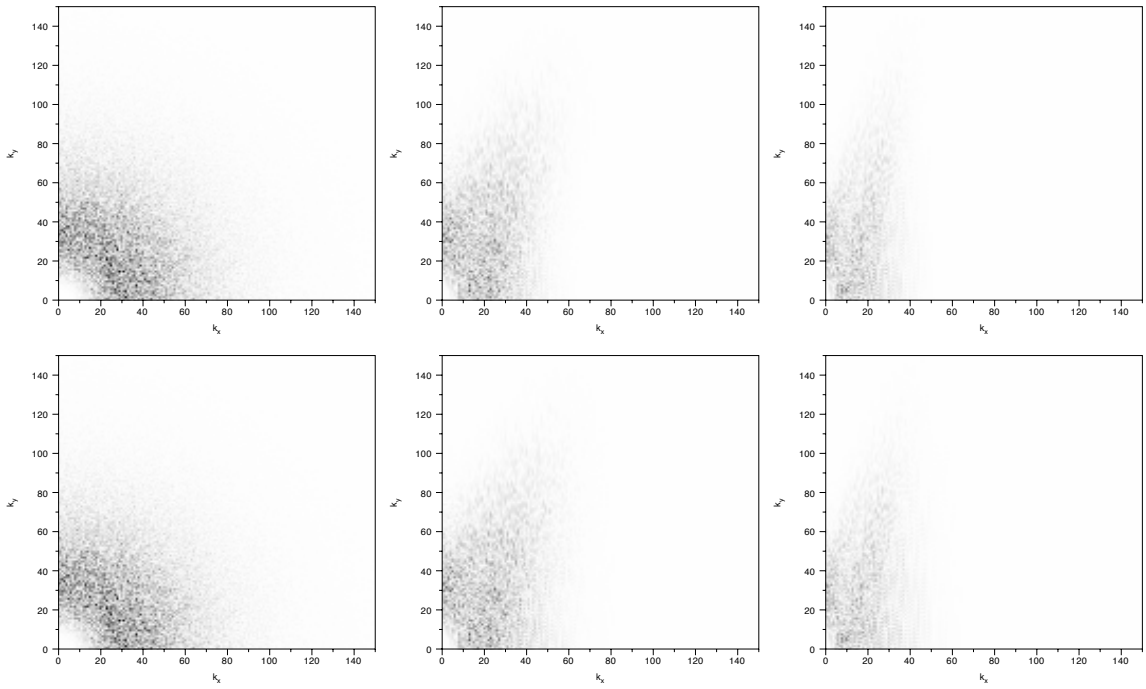

Figure 9, Camassa, Physics of Fluids

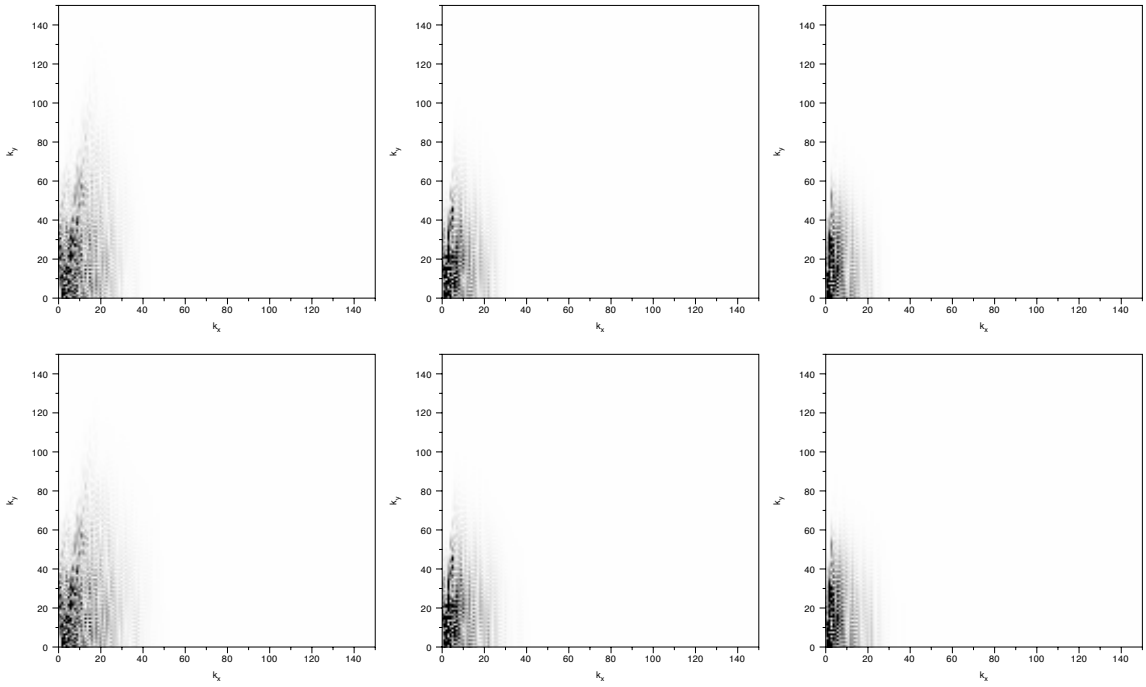

Figure 10, Camassa, Physics of Fluids

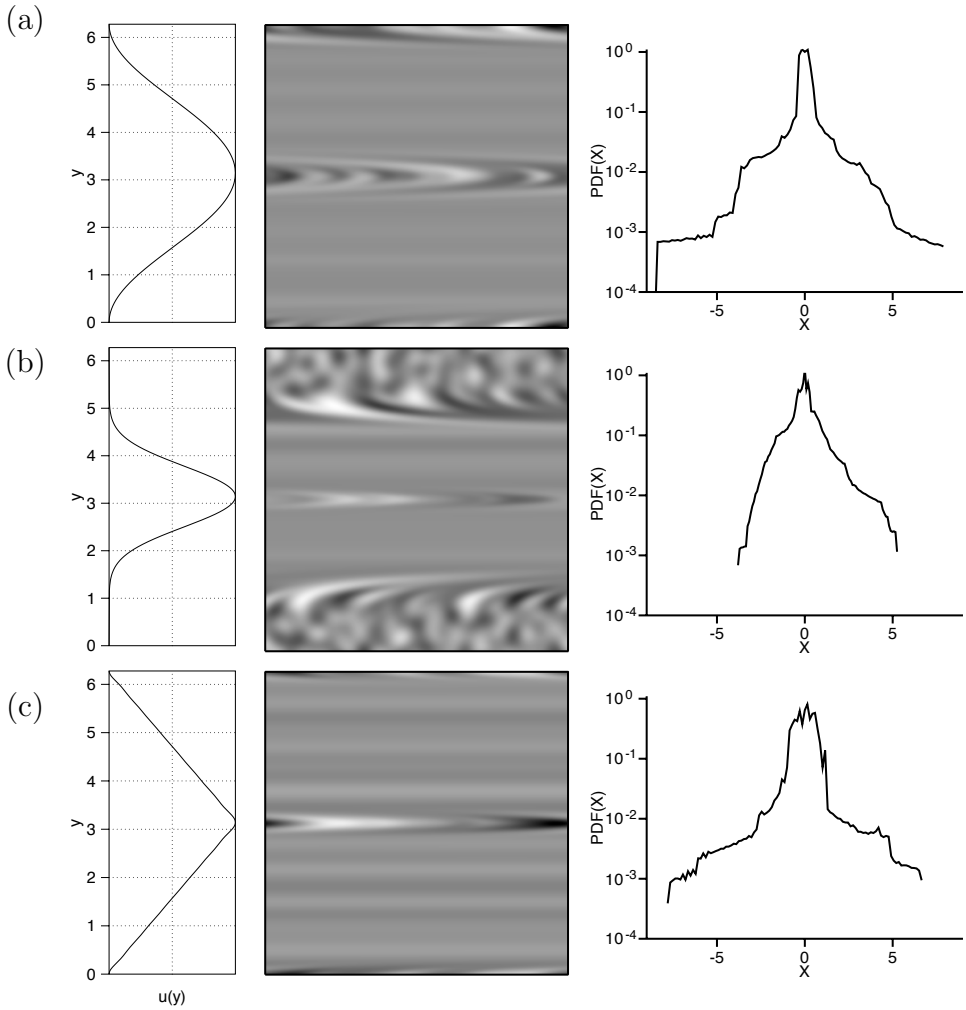

Figure 11, Camassa, Physics of Fluids

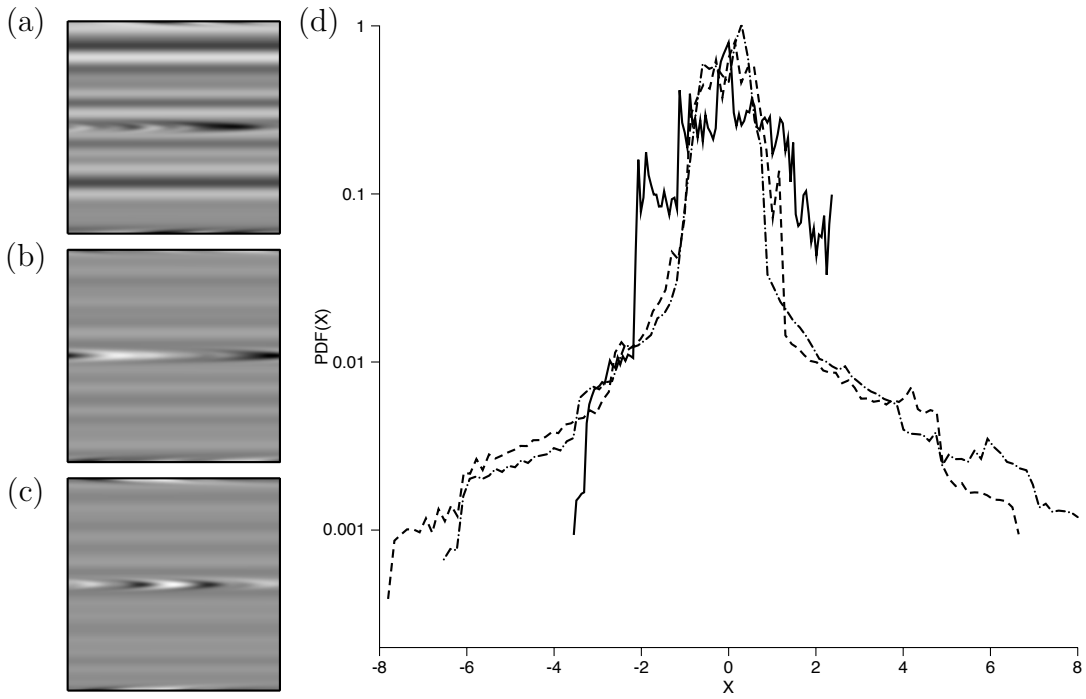

Figure 12, Camassa, Physics of Fluids

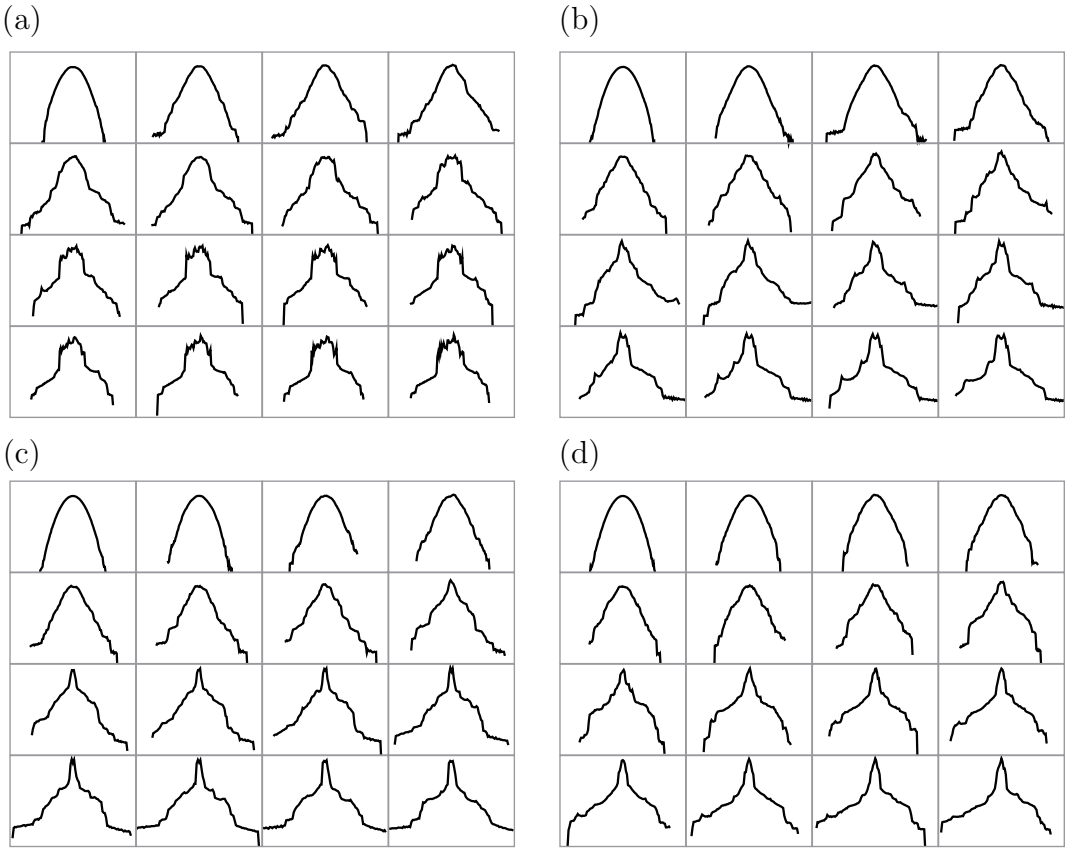

Figure 13, Camassa, Physics of Fluids

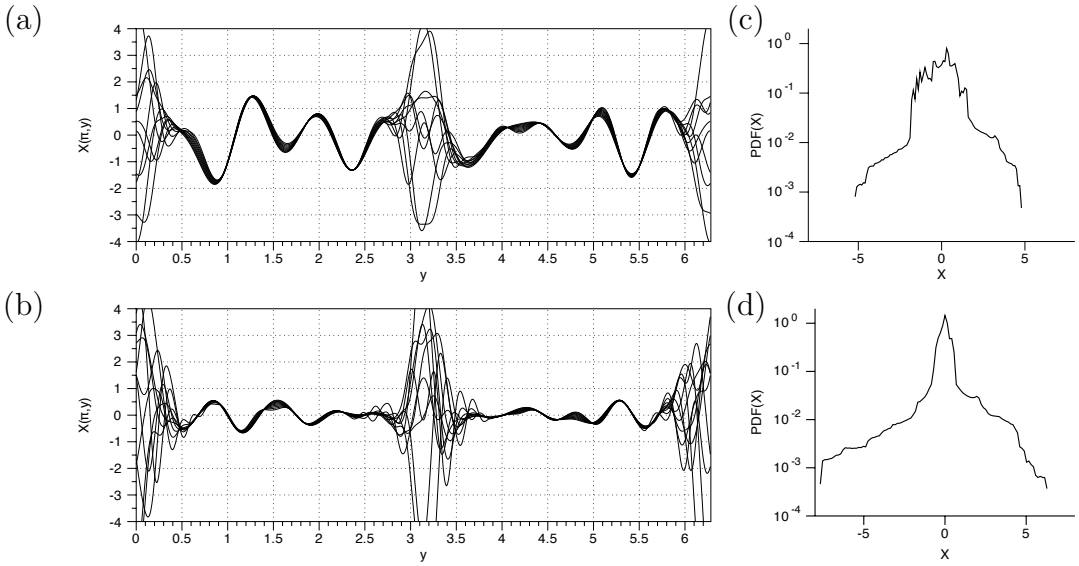

Figure 14, Camassa, Physics of Fluids

(a)

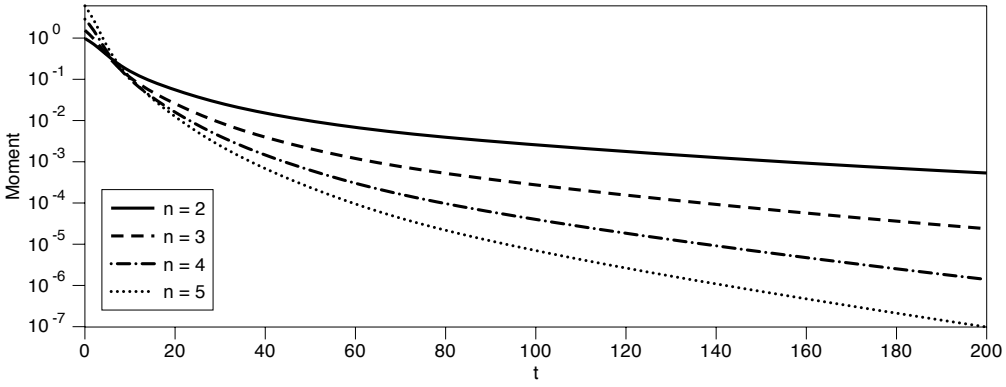

(b)

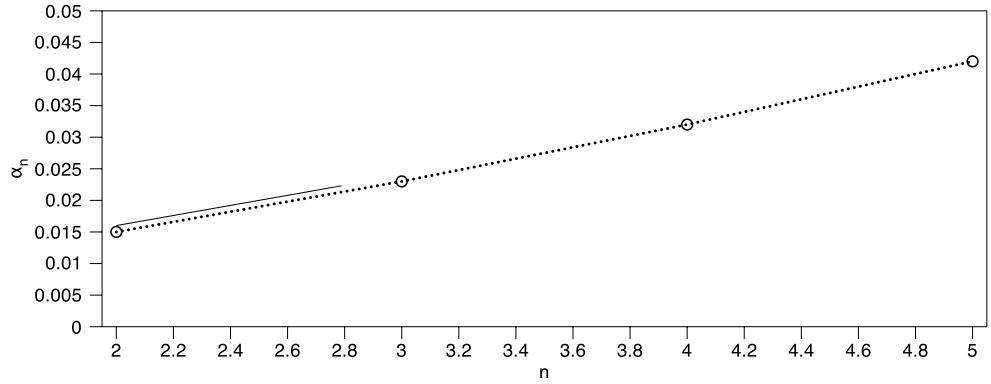

Figure 15, Camassa, Physics of Fluids

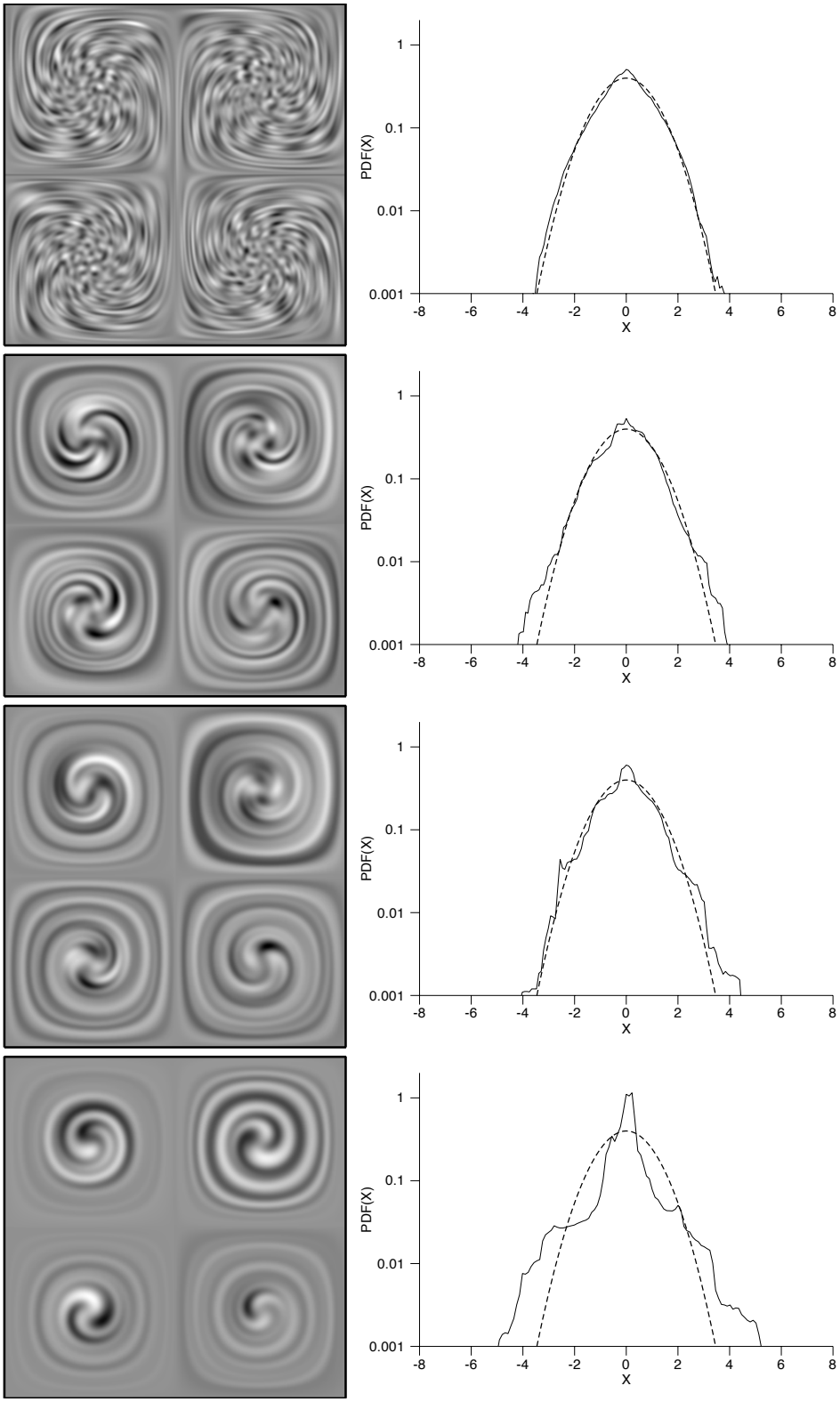

Figure 16, Camassa, Physics of Fluids

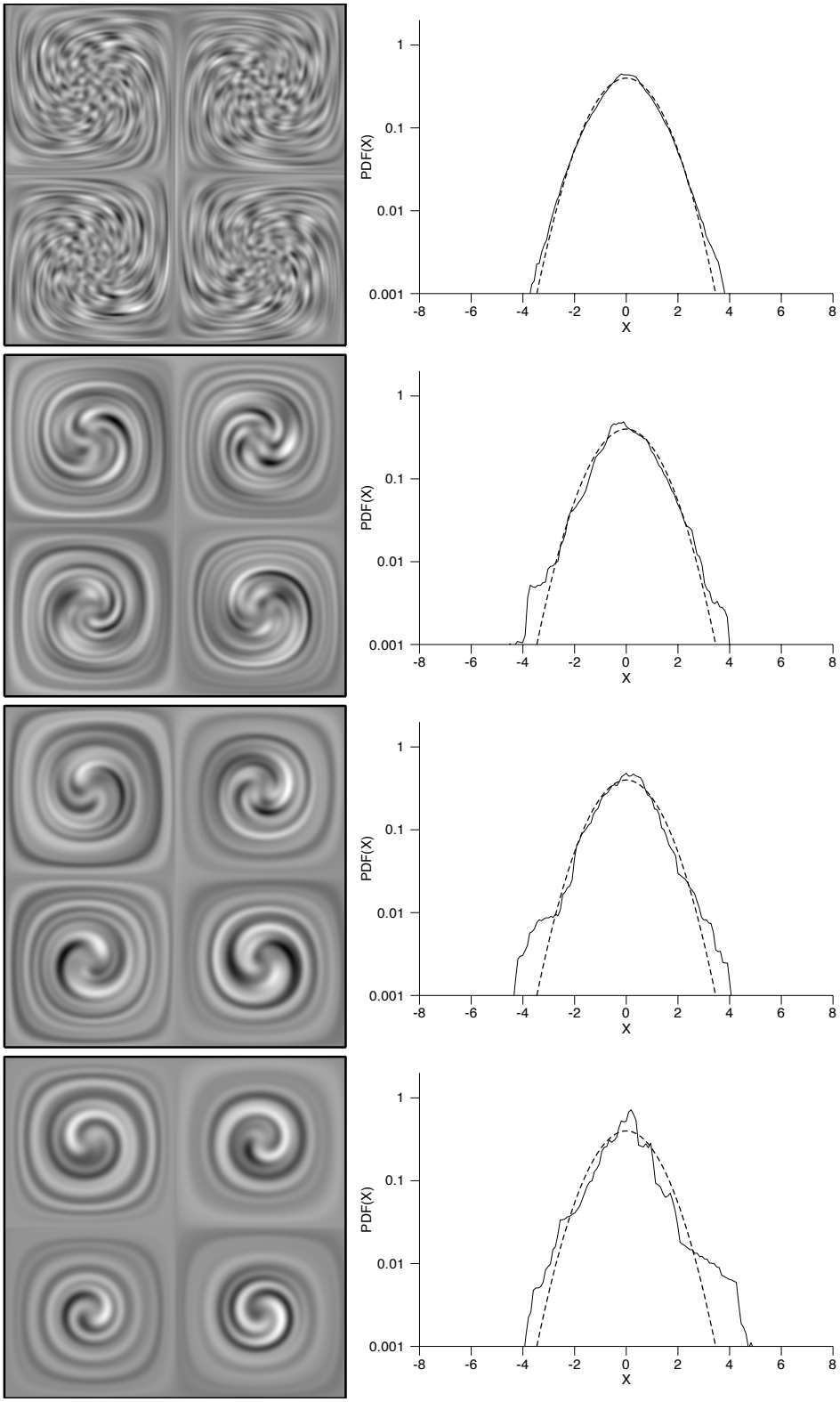

Figure 17, Camassa, Physics of Fluids

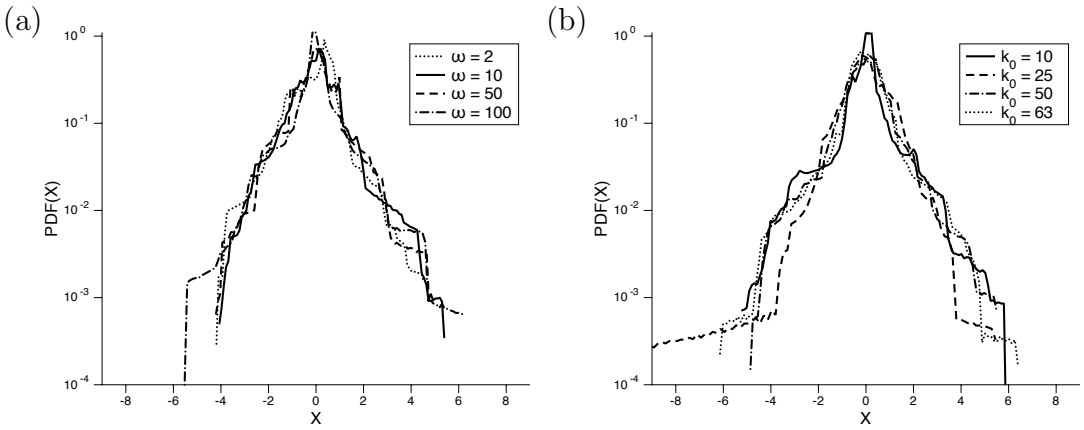

Figure 18, Camassa, Physics of Fluids

(a)

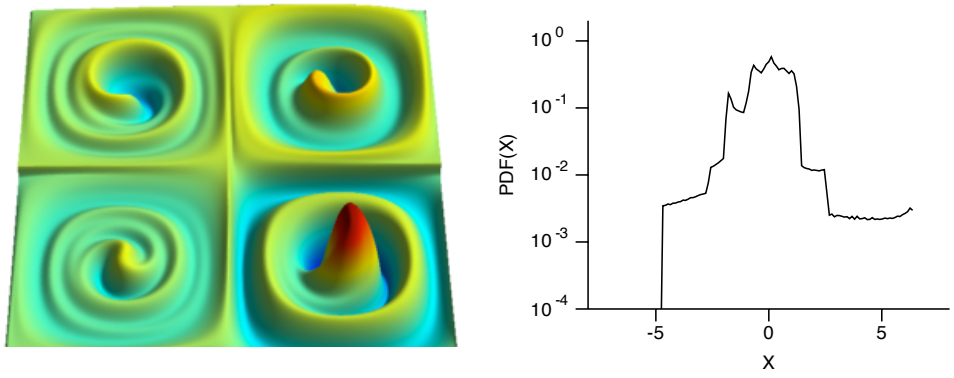

(b)

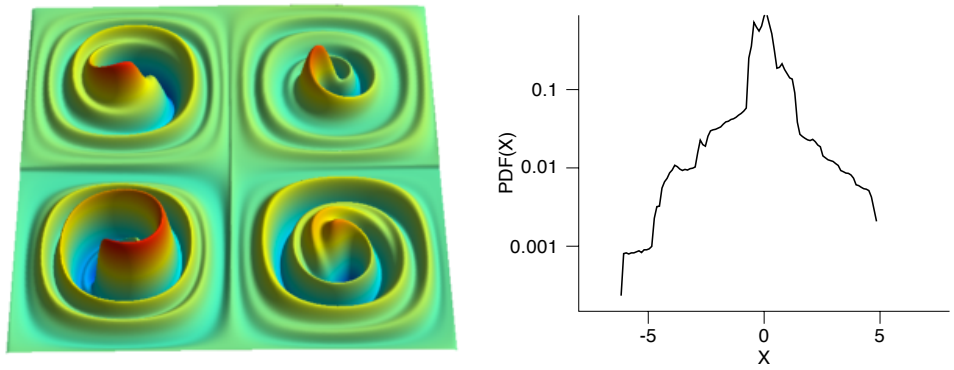

Figure 19, Camassa, Physics of Fluids

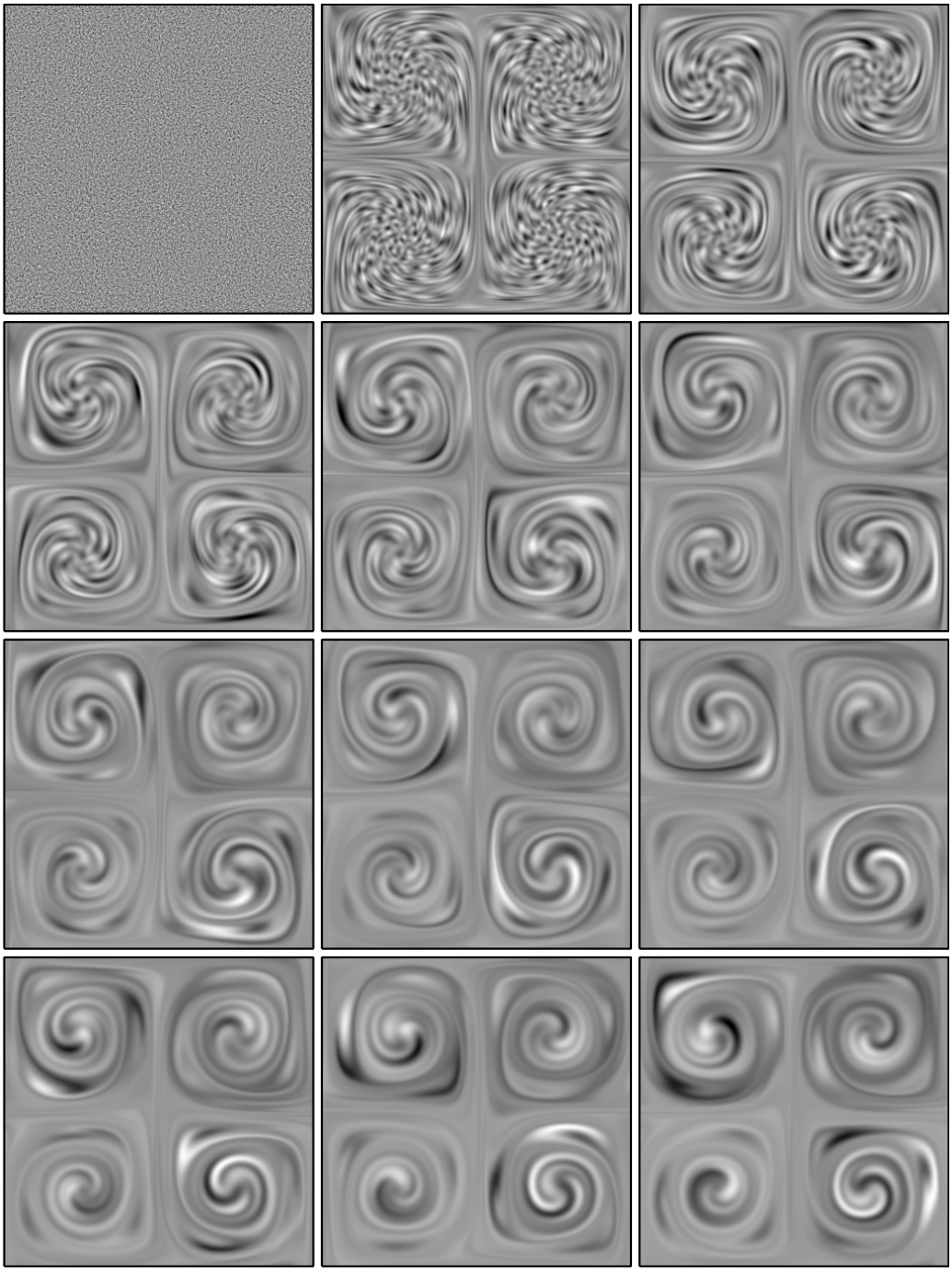

Figure 20, Camassa, Physics of Fluids

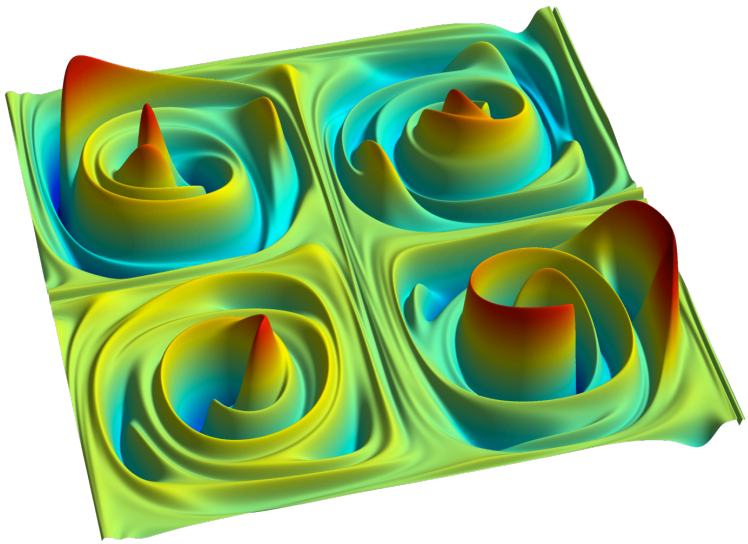

Figure 21, Camassa, Physics of Fluids

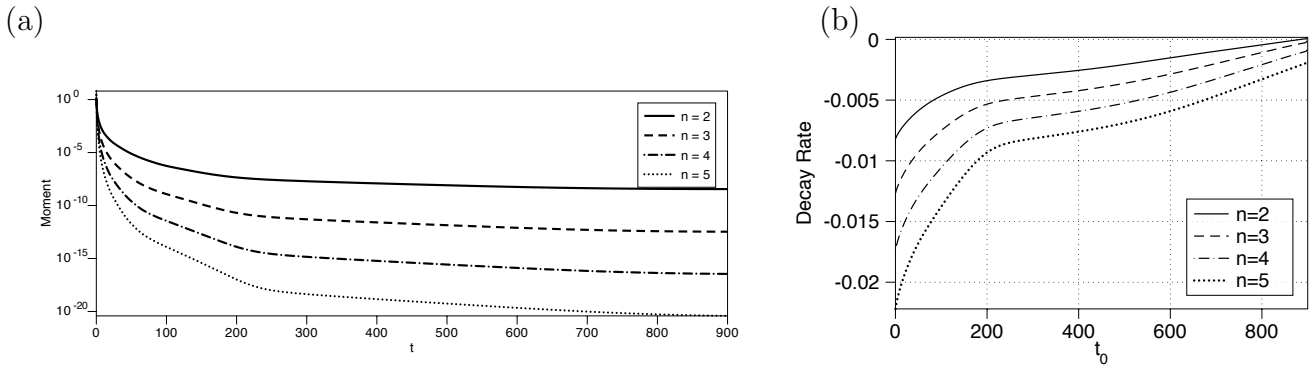

Figure 22, Camassa, Physics of Fluids

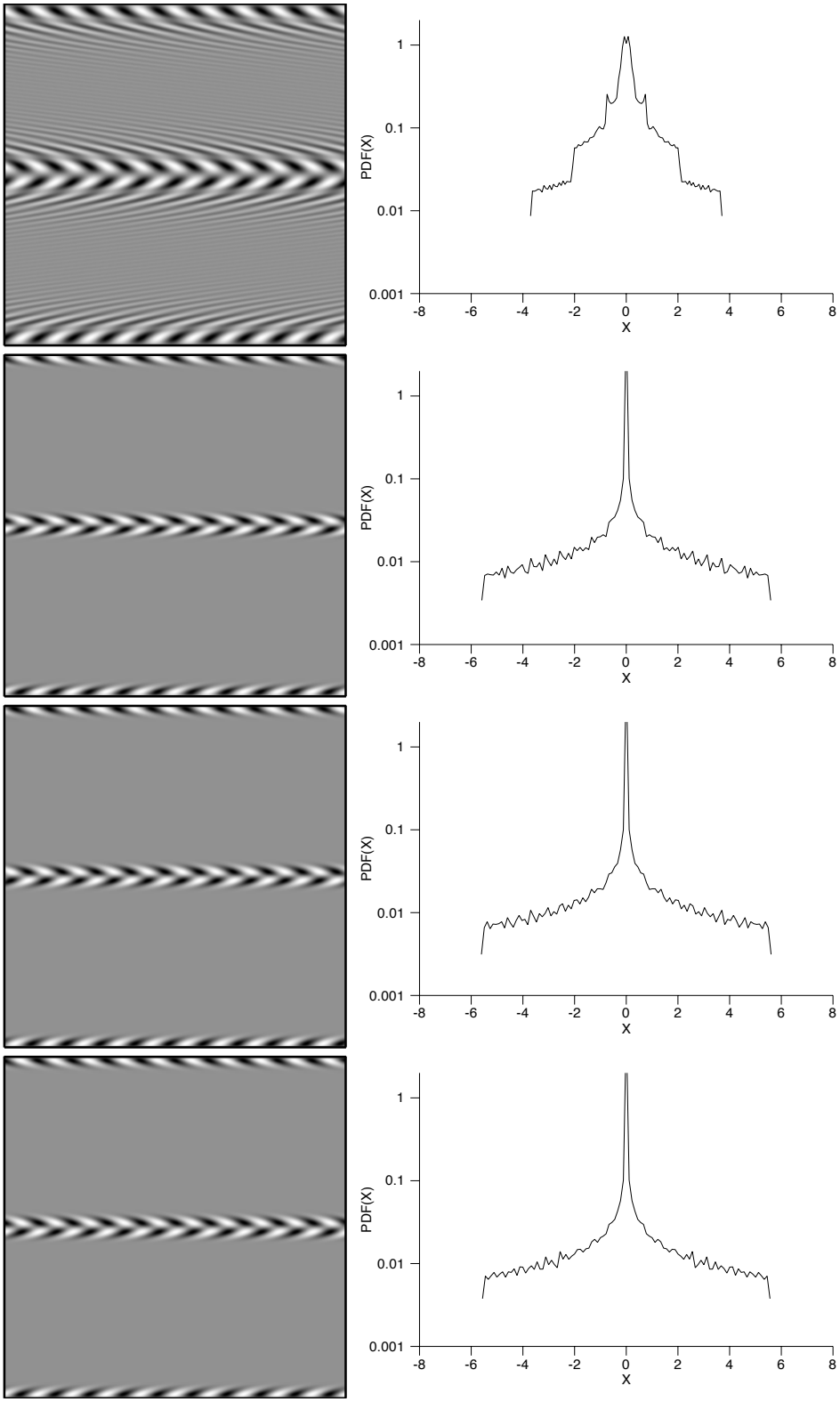

Figure 23, Camassa, Physics of Fluids

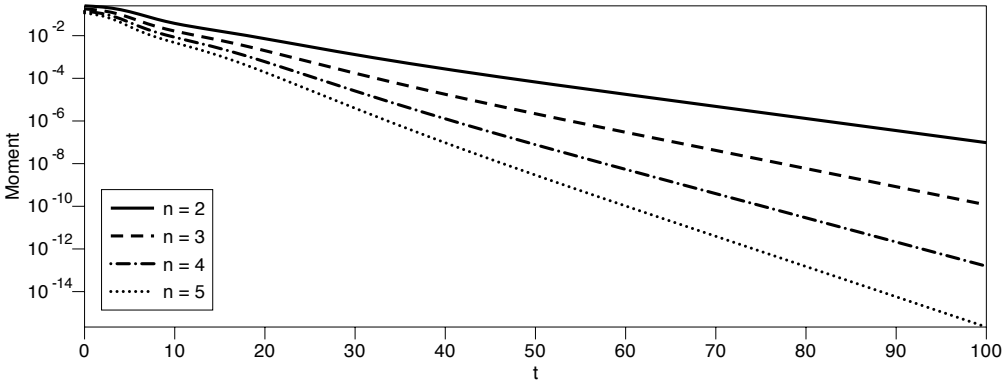

Figure 24, Camassa, Physics of Fluids

(a)

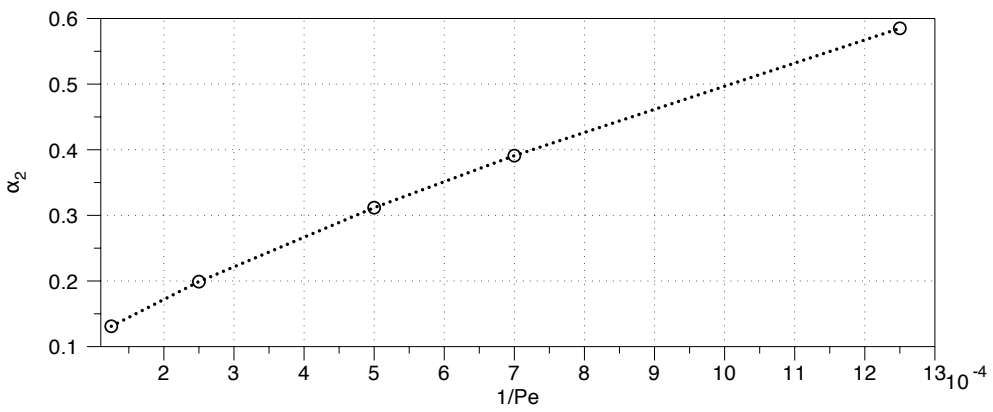

(b)

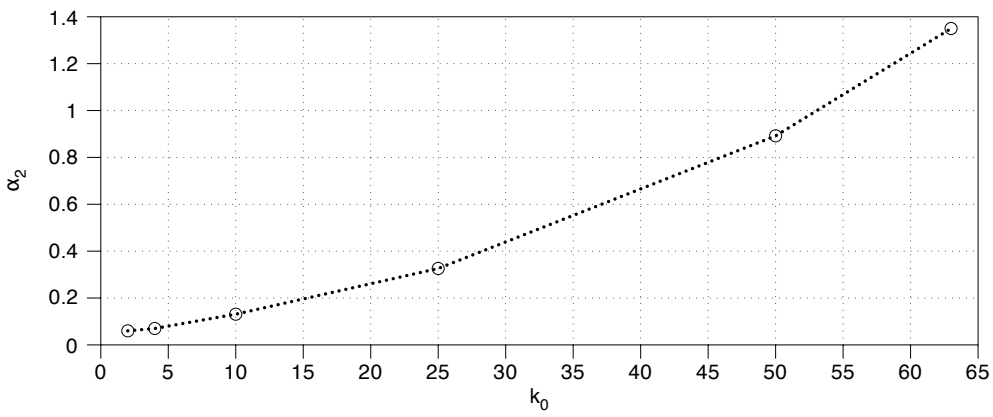

Figure 25, Camassa, Physics of Fluids

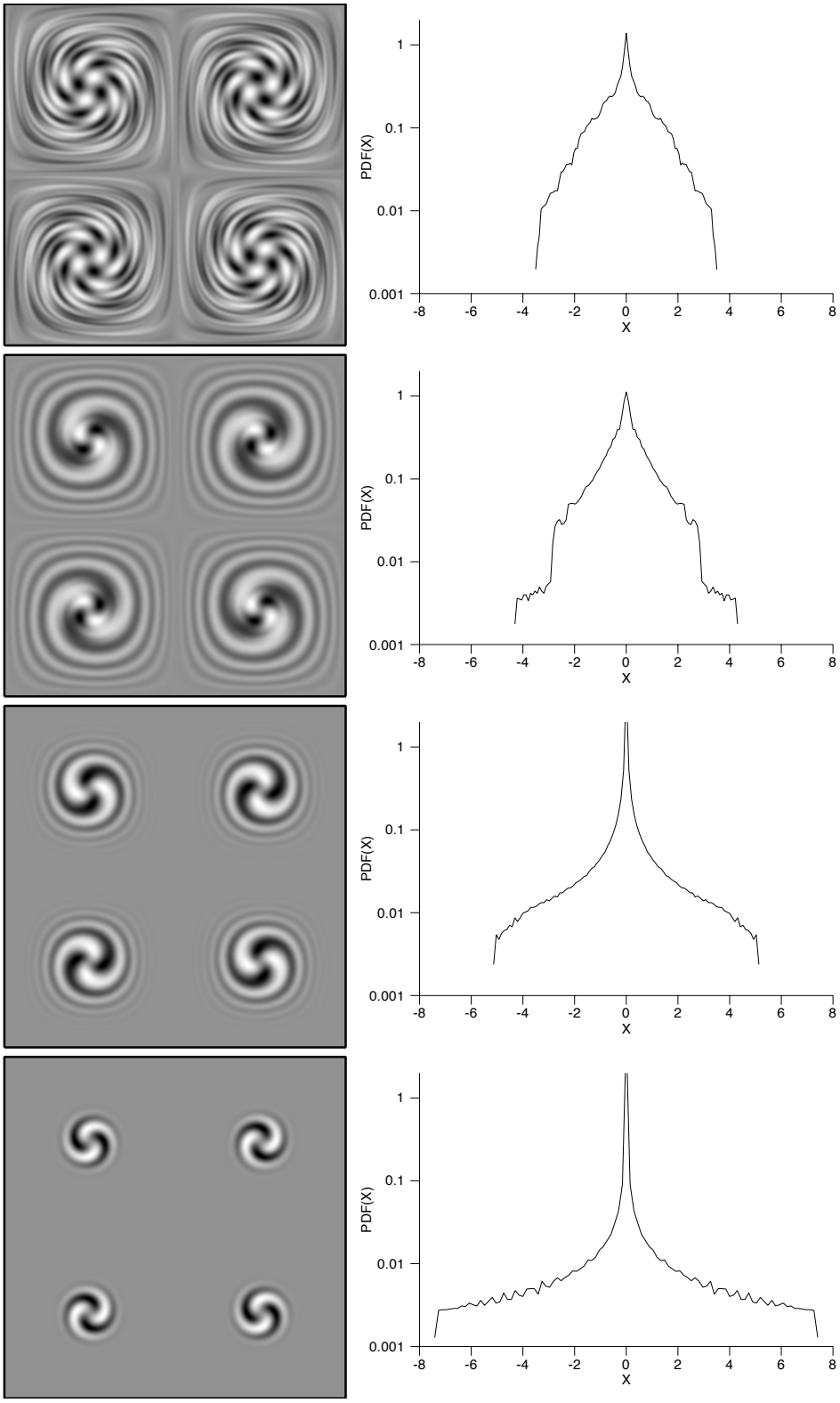

Figure 26, Camassa, Physics of Fluids